A Promethean Construct

Formulation of a bioink with human donor-derived liver dECM & liver Organoids

Flora Guarnotta

A Promethean Construct

Formulation of a bioink with human donor-derived liver dECM & liver organoids

by

Flora Guarnotta

to obtain the degree of Master of Science
in Biomedical Engineering,
at the Delft University of Technology,
to be defended publicly on March 23, 2023

Student Number:	5256895
Supervisors:	Dr. J.J.F. Sleeboom - TU Delft
	Dr. L.E. Fratila-Apachitei - TU Delft
	Prof. A.A. Zadpoor - TU Delft
	Dr. M.M.A Verstegen - Erasmus MC
	Prof. L.J.W. van der Laan - Erasmus MC
Project Duration:	February, 2022 - January, 2023
Faculty:	Faculty of Mechanical, Maritime and Materials Engineering, Delft

TU Delft

Erasmus MC
University Medical Center Rotterdam

Acknowledgment & Personal Reflection

Five years ago, I started my studies in Biomedical Engineering with the goal of improving people's lives through medicine. My bachelor's degree was focused on theoretical approaches and the use of image processing for diagnostics. I wanted to shift to a therapeutical approach of Biomedical Engineering, hence I applied to TU Delft with the aim of creating direct medical solutions. I became more interested in regenerative medicine (RM) and its potential to revolutionize healthcare. To pursue my strong interest in RM, I sought a master's graduation project with 3D bioprinting in the cytocompatibility (CCB) lab.

I would like to thank my supervisors Luc and Monique, who provided me with a fascinating master's thesis topic. The collaboration with Erasmus MC was very valuable for this research, as they generously supplied me with human donor-derived materials, rare for 3D bioprinting.

In comparison, to my previous projects, this one was the most challenging. I started the project with very limited knowledge of the wet lab, however, I was highly motivated to learn and gain technical knowledge. Some difficulties of this project arose from introducing a new research branch in the Biomaterials and Tissue for Biomechanics Department at TU Delft, focusing on the liver and human donor-derived materials. Through my master's thesis, I established protocols for ink formulation and organoids cultivation at TU Delft. Despite many setbacks delays, failures, and unpredictable responses, giving up was never an option. These challenges developed my mental strength and perseverance.

Facing these barriers would not have been possible without my daily supervisor, Jelle. He stood by my side every day and believed in me during the entire process. Jelle trained and helped me with manual manipulation. In addition to his help with the experimental work, Jelle dedicated a significant amount of time to improving my scientific writing skills. I was extremely fortunate to have such a supportive supervisor providing me with guidance and mentorship. I am incredibly grateful for his contribution which was essential to this project.

I would like to thank Lidy, my main supervisor for trusting me by including me in the CCB lab. Lidy is a passionate researcher, who was inspired by the project. She provided recommendations whenever my tests failed. Additionally, her rigorous standards and strict requirements challenged me to write and illustrate my reports in an insightful manner, encouraging me to exceed my expectations.

Maria, our laboratory technician was always present to assist me with any issues I encountered. She was essential in this project, as she taught me the fundamentals of cell culturing techniques, ranging from pipetting to staining techniques. Without her, I would not have been able to conduct any cell work or know about my astrological compatibilities. Furthermore, I would like to express my gratitude to all the people I met at the Erasmus MC and TU Delft, all curious and involved in my project. The positive work environment impacted my appreciation for this graduation project.

Finally, and most importantly, I would like to acknowledge all my family and friends. Throughout the project, they were always present, and supported me, even during my lowest moments. Without their care and advice, I would not have finished this master's degree in a healthy state.

In conclusion, regardless of the challenges and the extended duration of this project, I foresee myself continuing in working within the RM field. I consider myself privileged to have had the opportunity to work on this project, which provided me with invaluable knowledge and skills.

Flora Guarnotta
Delft, March 2023

Abstract

Liver diseases account for two million deaths worldwide each year, and current treatments are limited. 3D bioprinting is a promising technology, that has recently been investigated to tackle this challenge. However, the cells and hydrogels used for bioprinting are not human-derived and do not replicate the natural *in vivo* environment. The goal of this study was to develop a printable and cytocompatible liver bioink incorporating human donor-derived biomaterials, including liver decellularized extracellular matrix (dECM) and intrahepatic cholangiocyte organoids (ICOs).

The ink was formulated by using a first enzymatic crosslinking step with hydrogen peroxide (H_2O_2), horseradish peroxidase (HRP), and tyramine-modified hyaluronic acid (HAT), followed by a second crosslinking step with Eosin Y (EO Y). The concentrations of materials were altered to optimise the ink's printability evaluated with shape fidelity measurements. The printed scaffolds retained their structural integrity for three days in AdvDMEM/F12 medium. The stiffness of the scaffolds was comparable to healthy liver tissue based on compression tests. The ICOs viability was assessed in the formulated bioink, and the composition of the bioink was adjusted to improve its cytocompatibility. It was found that EO Y and H_2O_2 at concentrations of 0.01% v/v and 0.85 mM, respectively, were cytotoxic to ICOs. Nevertheless, ICO viability was demonstrated over three days in a bioink consisting of HAT and liver dECM.

The novel bioink showed promising results for creating a human donor-derived bioink for 3D bioprinting liver tissue. Further optimisation is required to enhance the printability of the bioink, and additional tests are necessary to evaluate the effect of the bioink's materials on ICOs. This bioink has the potential to be applied for liver disease modeling and drug development.

Abbreviations & Nomenclature

2D	Two-Dimensional
3D	Three-Dimensional
AdvDMEM/F12	Washing Buffer for intrahepatic cholangiocyte organoid
ANOVA	Analysis of Variance
BME	Basement Membrane Extract
dECM	Decellularized Extracellular Matrix
DNA	Deoxyribonucleic acid
DS	Degree of Substitution
EBB	Extrusion-based bioprinter
EC	Endothelial Cells
ECM	Extracellular Matrix
EM	Expansion Medium for ICO
EO Y	Eosin Y
Erasmus MC	Erasmus Medical Center, Rotterdam
EthD-1	Ethidium Homodimer-1
GelMA	Gelatin methacryloyl
H_2O_2	Hydrogen Peroxide
HA	Hyaluronic Acid
HAT	Tyramine-modified Hyaluronic Acid
HRP	Horseradish Peroxidase
HSC	Hepatic Stellate Cells
ICO	Intrahepatic Cholangiocyte Organoid
LAP	Lithium phenyl-2,4,6-trimethylbenzoylphosphinate
NaCl	Sodium Chloride
PBS	Phosphate Buffered Saline
qPCR	Quantitative Polymerase Chain Reaction
RM	Regenerative Medicine
SEM	Starting Expansion Medium
SLA	Stereolithography
STD	Standard deviation
TU Delft	Technische Universiteit Delft
UV	Ultraviolet

Contents

1 Introduction

Liver diseases such as cirrhosis and liver cancer account for two million deaths worldwide each year [1]. Current treatments for these diseases are limited. In the case of end-stage liver disease, liver transplantation is the only curative treatment option. However, with the limited number of available donor organs, alternatives need to be found [2]. Regenerative medicine is a dynamic field for developing novel therapeutic strategies for liver diseases and aims to find new treatment options for diseases. Often, two-dimensional (2D) *in vitro* models or *in vivo* animal models are used for this. These models have limitations as they do not entirely mimic the human environment and do not recapitulate the functionality of the human liver. Therefore, the development of more sophisticated liver models is necessary.

A promising technology that might eliminate organ shortages by creating viable replacement organs is 3D bioprinting [3]. In 2019, full-scale cardiac ventricles with human cardiomyocytes were 3D bioprinted, exhibiting synchronized contraction and propagation of action potentials [4]. The methods employed for organ printing are also used for smaller-scale studies including drug discovery or developing liver disease models. Liver diseases are often associated with an increase in tissue stiffness which is caused by scarring [5, 6]. By adjusting the stiffness of the model, liver disease models can be fabricated and used to investigate the progression of diseases and develop drugs, particularly for evaluating drug toxicity and efficacy [7].

3D bioprinting is a state-of-the-art technology that enables the fabrication of 3D tissues. A common liver bioprinting technique is extrusion-based bioprinting (EBB) [8]. EBB involves the deposition of a bioink containing live cells and a hydrogel acting as a support material. Many hydrogels have been explored for EBB, either derived from synthetic or natural polymers, the latter being preferred for biocompatibility. Gelatin, alginate, and gelatin methacryloyl (GelMA) are the commonly used natural polymers for liver bioprinting [9]. However, these materials are not derived from human tissues. Hyaluronic acid (HA) has been studied as a hydrogel material since it is a major component of the extracellular matrix (ECM) and for its natural presence in the liver. Tyramine-modified hyaluronic acid (HAT) hydrogels have been introduced as a biomaterial for their crosslinking capacity thanks to the addition of a tyramine functional group [10]. HAT hydrogels have been investigated to create bioprinted scaffolds with controllable mechanical properties for fabricating liver disease models [11]. Furthermore, researchers have shown that by adding alginate and Ca^{2+} to a HAT hydrogel, stiffness change can be induced over time [12]. These models could serve to understand the role of tissue stiffness in liver disease, and help to develop more effective therapies.

Cells alone reside in ECM as a 3D support structure [13]. ECM acts as a structural scaffold essential for cell function, signalling, and development [14]. Therefore, researchers have been investigating incorporating ECM into bioinks in the form of decellularised extracellular matrix (dECM) [15]. Liver dECM is obtained from the human liver by washing out the cells, leaving only the structural proteins such as collagens, proteoglycans, and laminins [14]. Scaffolds made from dECM retain organ-specific cues that have been shown to improve cell viability over time and induce cell differentiation [16–19].

The addition of dECM into GelMA bioink enhanced printability relative to pure GelMA [17]. Furthermore, dECM scaffolds have demonstrated increased mechanical stability under shear stress in comparison to alginate scaffolds. The study also demonstrated that dECM scaffolds kept their structural integrity for up to seven days [20]. To this day, the majority of dECM bioinks for EBB have been formulated by combining dECM with conventional hydrogels such as gelatin, alginate, and GelMA [21–23]. Studies with dECM bioink mostly used animal-derived dECM sources. A fully human donor-derived bioink needs to be developed for human application [24–26].

Most of the previous studies on liver bioprinting employed cell lines such as HEPG2 and HepaRG, usually originating from animal species or cancerous tissues as they have well-established protocols. However, these cell lines lack liver-specificity and cell-cell interactions essential for maintaining liver-specific functions and tissue-specific cellular processes [27]. The liver-specificity is required for studying liver physiology and pathology [28]. To address this limitation, co-culturing native liver cell types would be a more relevant approach.

Recently, liver organoids have been investigated as an alternative, as they are 3D cell structures that can self-organise through cell-cell and cell-matrix interactions [29]. These cells are highly proliferative, genetically stable, and can be cultured long-term. Liver organoids can better replicate native liver as they are grown in 3D environments [13]. Protocols are being developed to differentiate organoids into cholangiocytes, hepatic stellate cells (HSC), hepatocytes, and endothelial cells (EC) providing a similar liver phenotype that may replicate liver tissue [30]. Co-culturing these differentiated cells is essential for developing liver disease models, as fibrosis is involved in a complex interaction between hepatocytes, HSC, and EC [31]. In the future, organoids have the potential to improve the current *in vitro* liver models. When compared to cell lines, liver organoids are derived from human donors, which offers the possibility for transplantation.

Only two studies have integrated organoids with 3D bioprinting technology [32, 33]. In 2021 a toxicity study was published, where organoids were incorporated in a GelMA bioink and bioprinted with an EBB [32]. In another study, volumetric bioprinting was employed to bioprint organoids. This study demonstrated a high viability and morphology preservation of the organoids [33]. Liver organoids are a good candidate for EBB bioinks, yet they have not been extensively investigated. Further investigation is required to determine the potential benefits of liver organoids for bioprinting liver tissue.

To this day, no research has been conducted on bioinks consisting of human donor-derived liver dECM and liver organoids. These biomaterials should be investigated for their liver-specific functionalities, which would be a step closer to mimicking the liver *in vivo* environment [33]. Additionally, human-derived materials could offer the potential for tracking the progress of patient-specific diseases and fabricating personalised medicine. The objective of this study was to develop a novel liver bioink using human donor-derived liver intrahepatic cholangiocyte organoids (ICOs) and a hydrogel composed of HAT and liver dECM, suitable for extrusion-based bioprinting applications.

HAT hydrogels were made with a dual gelation process. A first crosslinking method to obtain a viscous hydrogel was triggered by an enzymatic reaction with horseradish peroxidase (HRP), hydrogen peroxide (H_2O_2), and HAT. An extrusion-based bioprinter was employed for its extensive range of available parameters and for its ability to print with a wide range of materials, demonstrating versatility. After the first crosslinking step, the hydrogels were placed in the EBB and extruded with a controlled pneumatic extrusion-system. The high-precision deposition x-y-z system deposited the hydrogels following a pre-determined toolpath. 3D scaffolds were fabricated by the addition of layers to the previous layers. To retain structural integrity the scaffolds were photo-crosslinked post-bioprinting using Eosin Y (EO Y).

The main challenge in 3D extrusion-based bioprinting is to obtain a bioink that is both printable and cytocompatible, within the biofabrication window [3]. To address this challenge, the research was divided into two objectives. The first objective was to formulate a printable ink composed of HAT and dECM by altering the concentrations of the constituents of the ink. The printability was then assessed by evaluating the shape fidelity of the printed scaffolds. In addition, their mechanical properties were assessed. The second objective of the project was to investigate the viability of the ICOs in the previously formulated ink and to optimise the ink composition to achieve a cytocompatible bioink.

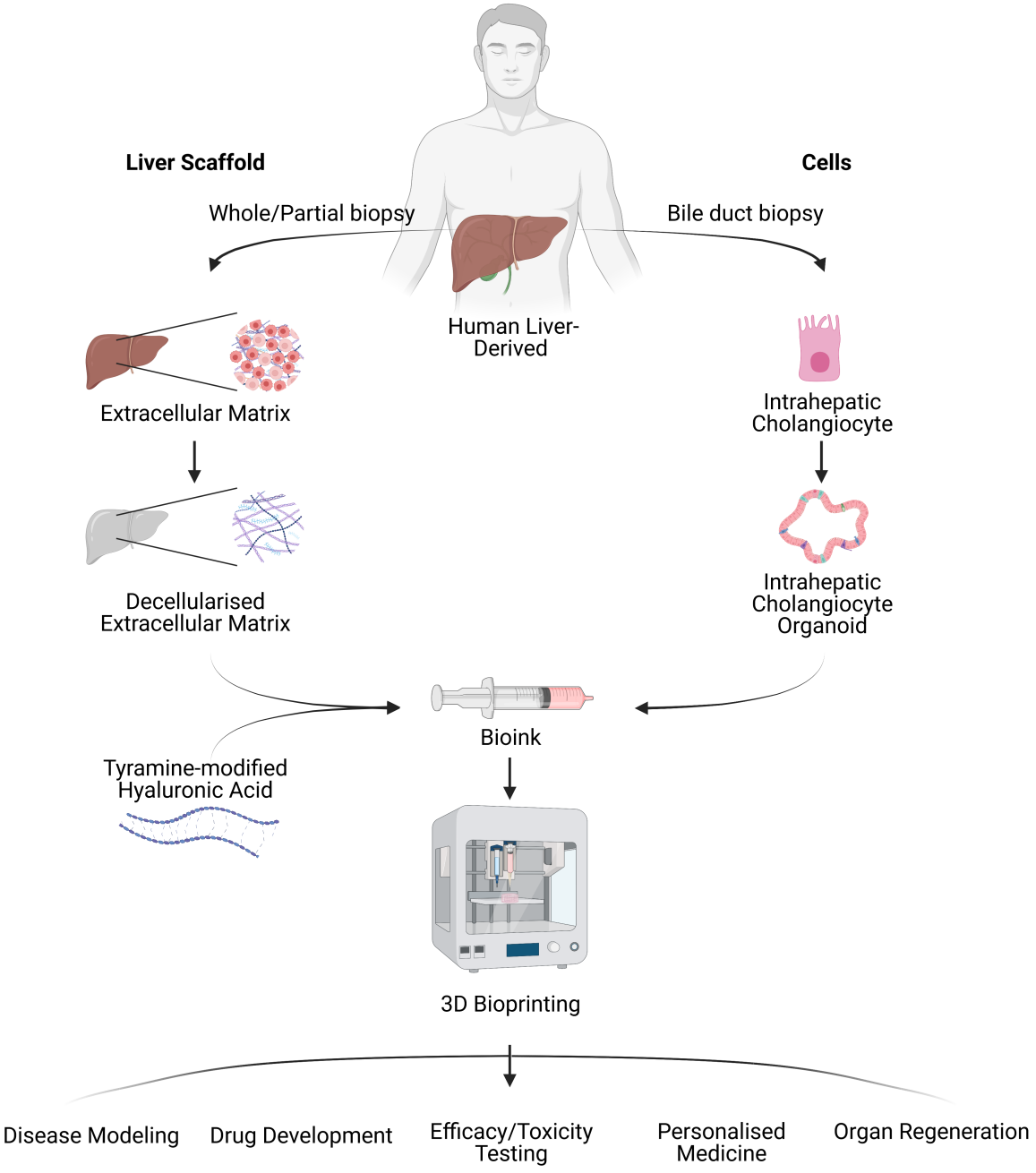

Figure 1.1: Graphical illustration of the process to formulate a bioink with liver human-derived dECM and organoid, along with examples of 3D bioprinting applications

2

Materials & Methods

2.1. Materials

The bioink was made with tyramine-modified hyaluronic acid with a molecular weight of 280-290 kDa and a degree of substitution of 6%. It was supplied by AO Research Institute Davos. The degree of substitution (DS) is a percentage representing the number of tyramine HA attached to the carboxyl group [10]. HRP (#516531-25KU), H_2O_2 (#216763-500ML), Eosin Y (#HT110232), and anti-collagen I anti-rabbit (#SAB4500362-100µg) were purchased from Sigma-Aldrich (St. Louis, Missouri, U.S.A.). Dulbecco phosphate-buffered saline (PBS) (#14200067), secondary antibody AlexaFluor 488 anti-rabbit (#A31627) and the Live/Dead^{TM} Viability/Cytotoxicity Kit (#L3224) containing Calcein-AM (#L3224A) and Ethidium Homodimer-1 (EthD-1) (#L3224B) were bought from Thermofisher (Waltham, Massachusetts, U.S.A.). Sodium Chloride (NaCl) (#A1671) was acquired from PanReac AppliChem (ITW Reagents, Milan, Italy). The human ICOs and human liver dECM were obtained from liver transplantation procedures at Erasmus MC Rotterdam. Erasmus MC provided the dECM made in 2019 from a batch of seven decellularised livers, based on a protocol established by Willemse J. [34]. The basement membrane extract (BME), the AdvDMEM/F12, the starting expansion medium (SEM), and the expansion medium (EM) were provided by Erasmus MC Rotterdam. The composition of the SEM, EM, and AdvDMEM/F12 can be found in Appendix A.

2.2. Methods

2.2.1. Organoid Culture

The organoids used for this project were donor-derived human intrahepatic cholangiocyte organoids provided by the Erasmus MC Rotterdam in frozen vials. The use of ICOs was approved by the Erasmus MC medical ethics committee.

ICO Initiation, Thawing

To start the ICO culture, BME was thawed on ice for at least two hours. A frozen ICO vial was quickly thawed in a 37^{o}C water bath until a little ice was left in the vial. Immediately after, in a biosafety cabinet, the ICOs were transferred into a 15 mL falcon tube and 900 µL of cold AdvDMEM/F12 was added. The cells were spun down (1500 rpm, 5 min, 4^{o}C) and the supernatant was removed. Based on the cell densities written on the frozen vial, the splitting ratio of the cells was determined. For example, if the frozen vial contained two domes with 70% confluency, it would be split with a 1:3 ratio resulting in six plated domes. The cells were carefully re-suspended avoiding any air bubbles in 25 µL of BME per well-calculated.

To prevent early gelation of the BME and facilitate the formation of domes in the wells, ice-cold P200 pipette tips were utilized to pipet 25 µL of BME containing the ICOs into each well of a 48 suspension well plate (#677102, Greiner Bio-One, Frickenhaussen, Germany). Suspension well plates were used instead of adherent well plates to ensure the ICOs would grow in 3D and not adhere to the bottom of

the well plate. To make sure the cells were evenly distributed in the gel, the well plate was inverted after 2-3 min, and placed in an incubator for 20-30 min at 37°C, 5% CO_2 to allow the BME to solidify. Next, 300 µL of warm SEM was added to the wells. After three days, the SEM was replaced by EM. The EM was refreshed every 2-3 days until the passaging of ICOs was required.

ICO Passage

ICOs were visually monitored and passaged every one to two weeks before the domes were over-crowded by the proliferating organoids, seen in Fig.2.1.

To prepare for the passaging of organoids, the BME was thawed on ice two hours in advance and the centrifuge (Sigma 4-16KS, Sigma) was pre-cooled to 4°C, the temperature at which the BME is in the liquid state. The expansion medium was first discarded from each well, followed by the mechanical dissociation of BME domes through pipetting and scraping 900 µL of cold AdvDMEM/F12 in each well. The solution was collected in a 15 mL falcon tube, and cold AdvDMEM/F12 was added until it reached a volume of 7 mL. The tube was placed in a centrifuge (1500 rpm, 5 min, 4°C) to separate and discard the supernatant from the pellet of ICOs. The ICOs were re-suspended using a 200 µL pipet with 3 mL of cold AdvDMEM/F12 and centrifuged another time. After the supernatant was removed, the splitting ratio was determined based on the density of ICOs in the domes. Usually, the ICOs were split 1:4 meaning that the organoids from one dome were split over four new domes.

The next steps were described in Section 2.2.1 and the ICOs were re-suspended in BME and plated. Instead of adding warm SEM to the well plate warm EM was pipetted in each well containing ICOs and refreshed every 2-3 days. The growth of ICOs in BME over three days can be seen in Appendix B.

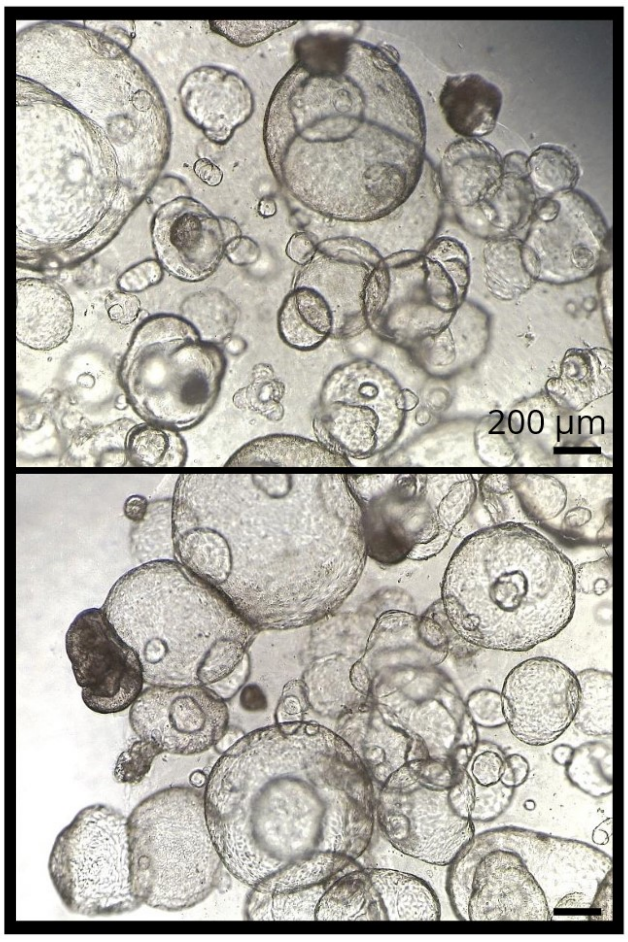

Figure 2.1: ICOs in BME ready for passaging. Scale bars 200 µm

2.2.2. Ink Preparation

In this project, the term ink refers to an acellular ink whereas the word bioink refers to the ink with the incorporation of organoids. Additionally, scaffolds describe a 3D printed structure using inks or bioinks. The ink formulation was based on work previously done [12, 35].

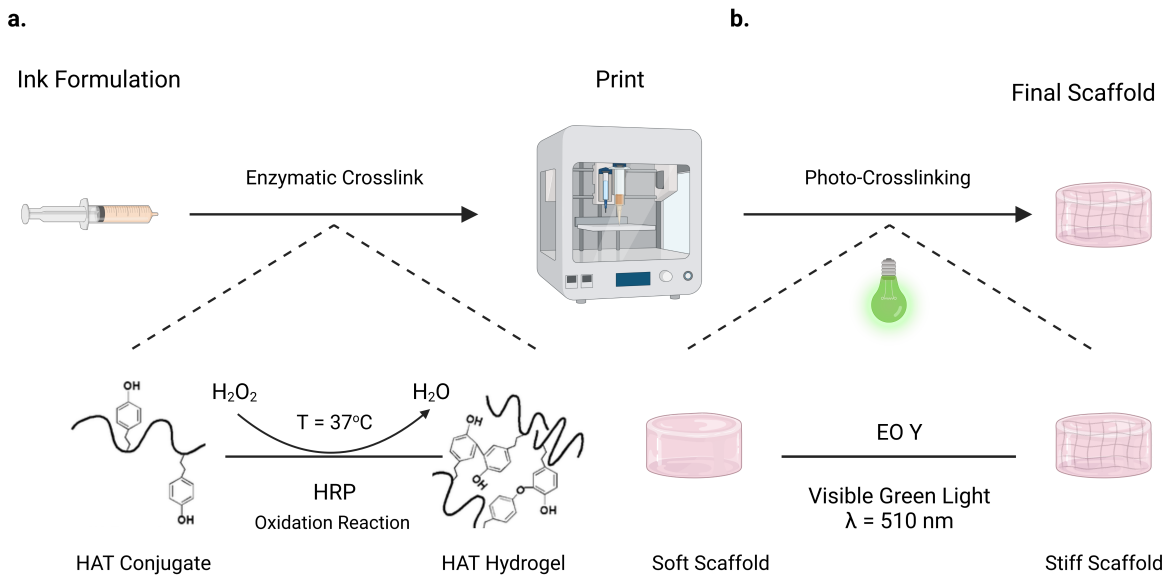

Figure 2.2: Graphical illustration of the HAT ink preparation for bioprinting with a dual gelation mechanism triggered by two crosslinking methods. a. Enzymatic reaction to crosslink the ink before printing, b. Photo-crosslinking of the scaffolds post-printing

HAT inks were developed with a dual gelation mechanism triggered with two independent crosslinking methods as shown in Fig.2.2. The first crosslinking method is an enzymatic reaction. This reaction occurs under similar conditions to the physiological environment with a neutral pH at 37°C. HRP is an enzyme used for crosslinking hydrogels due to its fast gelation, controllable crosslinking density, and non-toxicity. An oxidation reaction takes place with H_2O_2 and the HAT in the presence of HRP. From this reaction, H_2O_2 is consumed and transformed into H_2O forming a HAT hydrogel [36] [37]. This first reaction creates a hydrogel that has shear-thinning properties. Photo-crosslinking is the second crosslinking method employed for the scaffold to retain its structural integrity after printing. Eosin Y is added to the formulation of the bioink and its reaction is triggered when exposed to visible light ($\backsim$ 510 nm).

The novelty of the project was to introduce human donor-derived liver dECM in the ink. Table 2.1 indicates the different concentrations of HAT, HRP, H_2O_2, EO Y, and dECM that were used to create inks. The inks were prepared over two days, as seen in Fig.2.3.

On the first day, two 3 mL syringes (#309658, BD Plastipak), two female-to-female luer locks (#PSO030000502, CellInk), two lids for the syringes (#TP-MF-O, Boom B.V.), a balance (#AA-160, Denver Instrument), and a thermal shaker (#460-0249P, VWR) were required. The HAT powder was weighed and added in a 3 mL syringe with sterile NaCl 0.9%. HRP was added from the tip of the syringe while simultaneously pulling the plunger. A luer lock was used to connect the two syringes and thoroughly mix the components by passing the ink 100 times from one syringe to another. One syringe was disconnected and discarded while the other containing the ink, was protected from light with aluminium foil. The syringe was placed on a thermal shaker rotating at 300 rpm, at 4°C, overnight.

Table 2.1: Table of the materials and associated volumes investigated in the study for achieving a printable, cytocompatible HAT / dECM bioink

Material	Stock Solution	Acellular Ink	Bioink	Final Concentration
HAT	DS 6%	60 mg	-	3% w/v
		100 mg	150 mg	5% w/v
H_2O_2	1 mM	340 µL	510 µL	0.17 mM
	3 mM	340 µL	510 µL	0.51 mM
	5 mM	340 µL	510 µL	0.85 mM
HRP	1 $U.mL^{-1}$	20 µL	30 µL	0.1 $U.mL^{-1}$
	3 $U.mL^{-1}$	20 µL	30 µL	0.3 $U.mL^{-1}$
	5 $U.mL^{-1}$	20 µL	30 µL	0.5 $U.mL^{-1}$
EO Y	1% v/v	20 µL	30 µL	0.01% v/v
		40 µL	-	0.02% v/v
dECM	20 $mg.mL^{-1}$	20 µL	30 µL	0.2 $mg.mL^{-1}$
		60 µL	-	0.6 $mg.mL^{-1}$
		150 µL	-	1.5 $mg.mL^{-1}$

Acellular - Ink Preparation

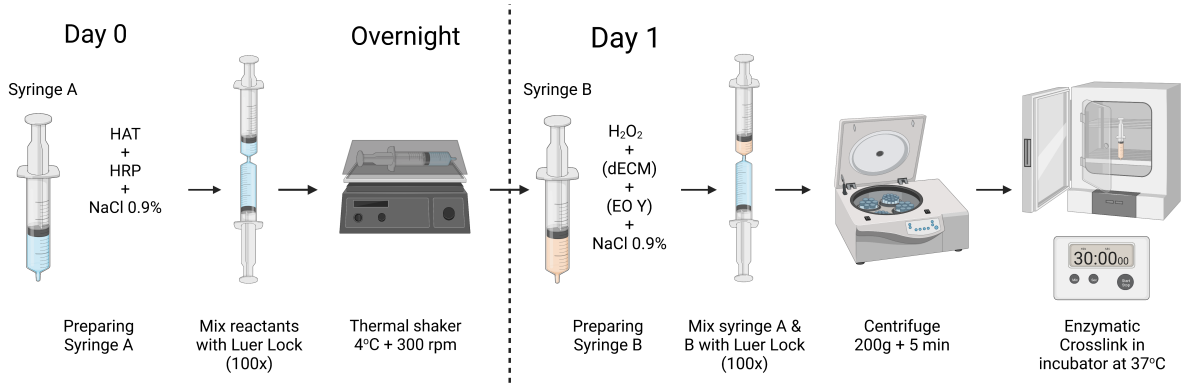

Figure 2.3: Graphical illustration of the ink preparation done over two days

To create the HAT and dECM inks, on the second day, the liver dECM had to be thawed at least one hour prior to finishing the ink preparation. The next day, a fresh batch of either 1, 3, or 5 mM of H_2O_2 was made by diluting H_2O_2 with sterile NaCl 0.9%. In a new 3 mL syringe, H_2O_2 and sterile NaCl 0.9% were added. EO Y was added from the tip of the syringe while simultaneously pulling the plunger. For the dECM ink, the decellularised extracellular matrix was added to the syringe in the biosafety cabinet after all the materials (H_2O_2, sterile NaCl 0.9%, and EO Y). The volumes added to the syringes are found in Table 2.1.

To bring all the components together, the H_2O_2 and EO Y containing syringe was connected with a luer lock to the HAT and HRP containing syringe. They were thoroughly mixed by passing 100 times the ink from one syringe to another. One syringe was disconnected and discarded. The other syringe containing the ink was placed facing up in a centrifuge for 5 min at 200g at room temperature to mix the components and separate the air from the ink. The air was removed by pushing the plunger of the syringe. To prevent early photo-crosslinking, the syringe was wrapped in aluminium foil and placed in the incubator at 37°C for 30 min. The syringe was incubated to initiate the enzymatic crosslink of the HAT, mediated with HRP and H_2O_2.

Bioink Preparation - Cellular

Similarly to the acellular ink, the preparation for the bioink required two days. This bioink required more steps and time as it had to be prepared under sterile conditions. Prior to the experiment the equipment, luer locks, and conical tips were autoclaved. The volume for the bioink preparation was increased by 1.5, to take into account the ink loss during sterile filtering.

On the first day, the HAT powder was weighed and put in the biosafety cabinet under the UV light for 20 min before introducing it in the sterile syringe. In a second sterile syringe, NaCl 0.9% and HRP were added, and a 0.2 µL sterile filter (#723-2520, ThermoScientific) was used to pass the solution into the syringe containing the HAT powder. The ink was mixed and placed on the thermal shaker.

The next day, in the same way as the acellular ink, fresh batches of different H_2O_2 concentrations were made. In the biosafety cabinet, H_2O_2, NaCl 0.9%, and EO Y were added to a 3 mL syringe based on Table 2.1. A 0.2 µL sterile filter was used to pass the solution into a new 3 mL syringe. The syringe with HAT and HRP prepared on the previous day was mixed with the EO Y and H_2O_2 syringe. The protocol was then identical to the acellular ink preparation. To reduce the effect of H_2O_2 on the organoids, the ink was enzymatically crosslinked before incorporating the ICOs.

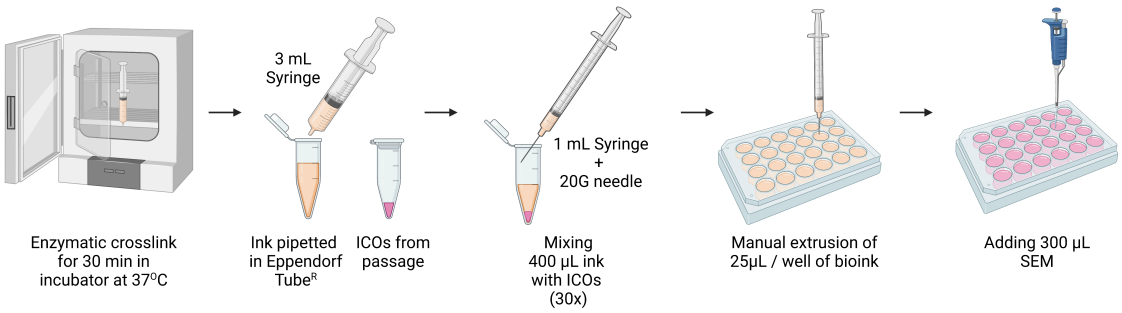

Figure 2.4: Graphical illustration of bioink preparation, with the incorporation of ICOs in the acellular ink

The next step was to incorporate the organoids in the ink. To achieve this, the ICO cultures had to be ready for passage. A BME dome containing ICOs at a 1:4 passage ratio yielded 100 µL of bioink. To obtain 400 µL of bioink, four domes were split following the procedure outlined in Section 2.2.1. When the supernatant was removed instead of adding 25 µL of BME per well, the sterile ink was carefully mixed with the ICOs. 400 µL of the ink was withdrawn using a 20G needle connected to a 1 mL syringe. Then, the ink was carefully deposited in a 1.5 mL Eppendorf Tube® (#3810X, Eppendorf) containing the organoid pellet and mixed slowly by pipetting up and down 30 times. This step required delicacy to avoid the introduction of shear forces and the formation of air bubbles. Once the organoids were mixed in the bioink, they were manually pipetted in a 24 well plate (#83.3922.500, Sarstedt) to create 25 µL domes. If the bioink contained EO Y, the well plate was exposed to the visible green light ($\backsim$ 510 nm) for 5 min on the top side and 5 min on the bottom side. The light was placed 3 cm from the well plate. Lastly, 300 µL of SEM was added to the wells and the well plate was placed in the incubator. The organoids were monitored by taking microscopic images on days 1,2, and 3.

2.2.3. Printing

Printing Process

An extrusion-based bioprinter, BIO X (CellInk) with a pneumatic printhead (#000000020340, CellInk) was used to print in this project. Before printing, some steps were required. The ink was passed twice through a 20G conical nozzle (#NZ4220005001, CellInk), to insure the homogeneity of the ink, and transferred to a UV-protected cartridge (#CSO010311502, CellInk). A piston (#PSO030000502, CellInk) was inserted in the cartridge and closed by an air adapter connector (#000000010040, CellInk). A 22G nozzle was mounted on the ink cartridge. The wide nozzle was chosen over narrower nozzles to limit the shear forces applied on the ICOs when extruded. The cartridge was placed in the pneumatic

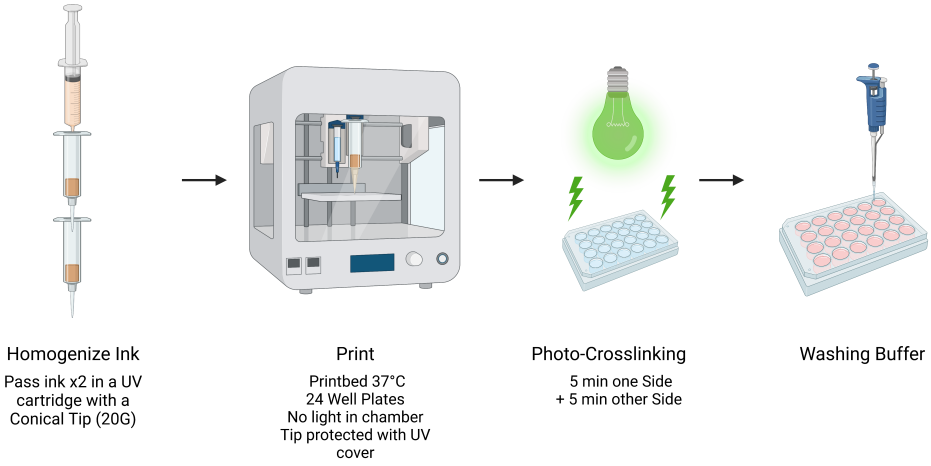

Figure 2.5: Graphical illustration of the printing process for the acellular ink

printhead of the printer. The GCode was uploaded to the printer.

The 3D scaffolds were printed inside the 24 suspension well plates on a printbed set to 37°C, to ensure stable crosslinks. This temperature was selected as the dECM gelation temperature is 15°C and raising the temperature to 37°C enables the formation of stable cross-links [15]. In addition, ICOs were kept in 37°C cultures to proliferate. The speed of the printhead ranged from 20-35 mm.s^{-1} and the pressure from 15-45 kPa.

After the scaffolds were printed, they underwent a post-crosslinking step, which consisted of exposing visible green light ($\backsim$ 510 nm) for 5 min on one side of the well plate and 5 min on the other side. AdvDMEM/F12 was added to the well plates, and a compression test could be followed. The well plates were stored in the incubator at 37°C.

2.2.4. Printing Design

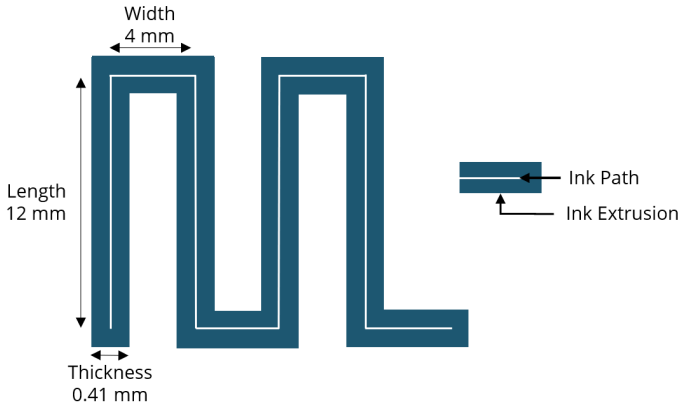

Figure 2.6: Top view of the design used for printing 2D lines with the associated dimensions

The designs were created with GCode in text file (.TXT) and imported in CAMotics (v.1.2.0) to visualise the result. The printing designs were based on printing patterns employed by the previous master students in the research group [38–40]. The 2D line design was a continuous line that was printed with 90°C angles, the length of the model was 12 mm and the width was 4 mm, seen in Fig.2.6. The design was chosen as it was the 2D base for the 3D printed scaffold.

Fig.2.7 shows the design that was used for creating the 3D scaffolds. The base of the scaffold used a similar pattern to the 2D line, but with altered dimensions. The base of the scaffold measured 4.8 mm x 4.8 mm. From one layer to another the pattern was rotated by 90°C, this method was used to

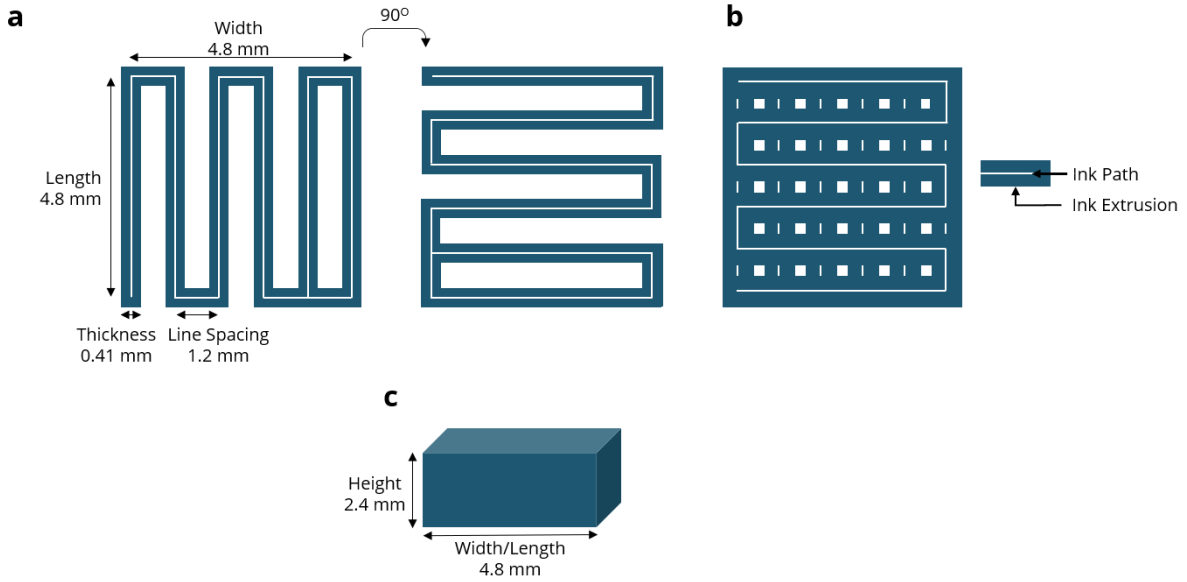

Figure 2.7: 3D design employed to print scaffolds. a. Top view of the toolpath used for printing the 3D printed scaffold. A rotation of 90°C was applied for each layer to create a stable 3D scaffold, b. Superposition of each consecutive layer, the white squares represent the unfilled spaces, c. Side view of the scaffold

create a 3D cube with 3 layers and a height of 2.4 mm.

2.2.5. Shape Fidelity

Shape fidelity is a measurement of the similarity between the print and the design. First, the percent error using the theoretical dimension from the GCode in comparison to the experimental value was computed and subtracted to 100. As described in Equation 2.1:

$$\text{Shape Fidelity [\%]} = 100 - \left(\frac{|GCode - exp.|}{exp} * 100 \right) \tag{2.1}$$

where $GCode$ represent the dimensions of the theoretical design model and $exp.$ the dimensions of the scaffold

2D Shape Fidelity

For the 2D shape fidelity two experimental values were taken: the length and width of the line, as shown in Fig.2.6. After taking pictures from the top of printed glass slides, the measurements for the 2D line were obtained with ImageJ software (v.1.52a). The length, width, and layer thickness were measured three times and averaged. The line thickness was not a parameter selected prior to printing. Therefore, it was chosen to be the inner diameter of the nozzle used. A 22G nozzle was employed resulting in an inner diameter of 0.41 mm.

3D Shape Fidelity

For the 3D shape fidelity, a digital caliper was used to measure the base area and the height of the scaffold. The dimensions of four scaffolds were taken for each ink.

2.2.6. Nozzle Protector

It was noticed that EO Y photo-crosslinked rapidly in the nozzle at the exposure of visible light, which led to the nozzle clogging. It prevented using the same pressure and printing speed from one well to another, where the scaffolds were not reproducible. Therefore, a nozzle protector was designed and 3D printed using a stereolithography (SLA) printer (Formlabs, v.3.18.0), seen in Fig.2.8.

Figure 2.8: UV nozzle protector installed on a pneumatic printhead for the BIO X (CellInk) Bioprinter

2.2.7. Immersion Test

To assess the structural stability of the scaffolds, an immersion test was conducted. The scaffolds were submerged in AdvDMEM/F12 after printing, representing the expansion medium employed for growing ICOs. The test was carried out over three days, during which the AdvMEM/F12 was removed and the scaffolds were inspected daily for any changes in their appearance. This duration was chosen to demonstrate that ICOs can be incorporated and monitored over three days. After the test was completed, the samples were refreshed with fresh medium and placed in the incubator.

2.2.8. Compression Test

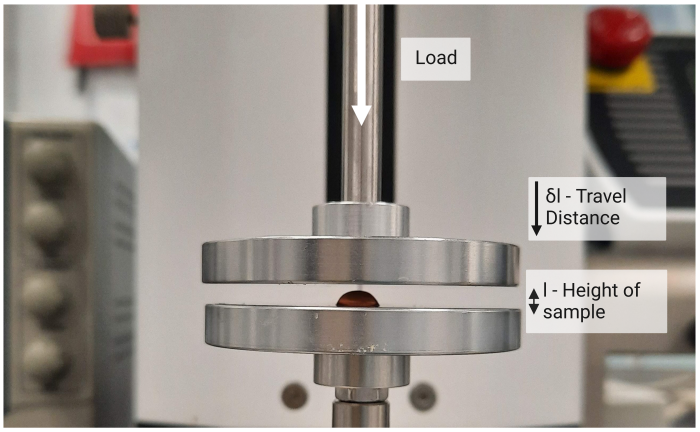

Figure 2.9: Compression Test of a 3D printed scaffold

A compression test to evaluate Young's Modulus was realised on four (n = 4) acellular scaffolds. Compression tests were performed for four inks on the day of printing. In addition, compression tests were performed on days 0, 1, and 2 for the ink selected for the incorporation of ICOs. To replicate the conditions with organoids, AdvDMEM/F12 was supplemented post-printing on the scaffolds simulating expansion medium.

The tests were performed using a motorized compression test stand (ESM303, Mark-10, Copiague, NY, US) equipped with a 2.5 N load cell and two 50 mm diameter parallel compression plates, seen in Fig.2.9. The scaffolds were compressed under the same condition. Prior to compression, the samples were removed from the well plate and their size (length x weight x height) was measured using a digital caliper. Under ambient conditions, the scaffolds were placed in the center of the plates and compressed at a speed of 1 mm.min^{-1}, and 15 recordings per second were taken. The scaffolds were compressed until 50% of the sample height was reached, (1.2 mm). The machine recorded the time (sec), force/load (N), and travel distance (mm). From this, the strain was calculated as the ratio between the height of the compressed sample (l-δl) and the original height of the scaffold (l), where δl is the travel distance of the plate. The strain (ϵ) and stress (σ) were calculated based on Equation 2.2, 2.3 with MATLAB (R2020b, Mathworks) :

$$\sigma = \frac{Load}{Area} \tag{2.2}$$

$$\epsilon = \frac{\text{l-}\delta\text{l}}{l} \tag{2.3}$$

To stay within the elastic part of the sample, Young's modulus was obtained by selecting 0 - 10% of the strain where the stress/strain curve was linear. A first-degree polynomial was fitted on the curves, the coefficients were computed representing Young's modulus for each ink. The equation for the strain is defined in Equation 2.4.

$$E = \frac{\sigma}{\epsilon} \tag{2.4}$$

2.2.9. Live/Dead Staining

The viability of the ICOs was measured on day 3, with a Live/Dead^{TM} Viability/Cytotoxicity Kit (#L3224). Live/Dead staining contains two materials: Calcein-AM which selectively colors live cells green and Ethidium Homodimer-1 (EthD-1) which colors dead cells red. Calcein-AM is a membrane permeable dye. The stain is activated with a wavelength of 494 nm. If the sample contains viable cells, Calcein-AM is hydrolysed with enzymes present in the membrane of the cells. The presence of cells was then imaged with green fluorescence at 517 nm. Whereas EthD-1 is a membrane impermeable dye, that becomes fluorescent once it is bound to deoxyribonucleic acid (DNA). The red fluorescence representing cell death is detected at 617 nm [41].

First, the expansion medium was removed and the wells were washed with 1x PBS, 2 times for 5 min, at room temperature. The staining solution was made by adding 2 mL of 1x PBS, 3 µL of EthD-1, and 1 µL of Calcein AM to 2mL of 1x PBS. 400 µL of the staining solution was added to each well and incubated at 37°C for 1 hour. The samples were imaged with the green and red channel of the Zoe Fluorescent Cell Imager (BioRad, Hercules, California, U.S.A.)

2.2.10. Statistical Analysis

The results were presented as the mean value and $\pm$ standard deviation (STD). Statistical analysis was applied on quadruplet for each condition and performed with MATLAB. A one-way analysis of variance (ANOVA) was used for comparing multiple groups of data with the same variable of interest. For parametric data, a two-sample t-test was used. For non-parametric data, where the data did not have a probability distribution a Wilcoxon signed-rank test was used [42]. All the tests were considered statistically significant when *:p $\leq$ 0.05.

2.2.11. Overview of the Performed Experiments

The tests conducted throughout this research are shown in Fig.2.10. The compression and collagen stainings were done on printed acellular scaffolds. All the tests containing ICOs were manually extruded.

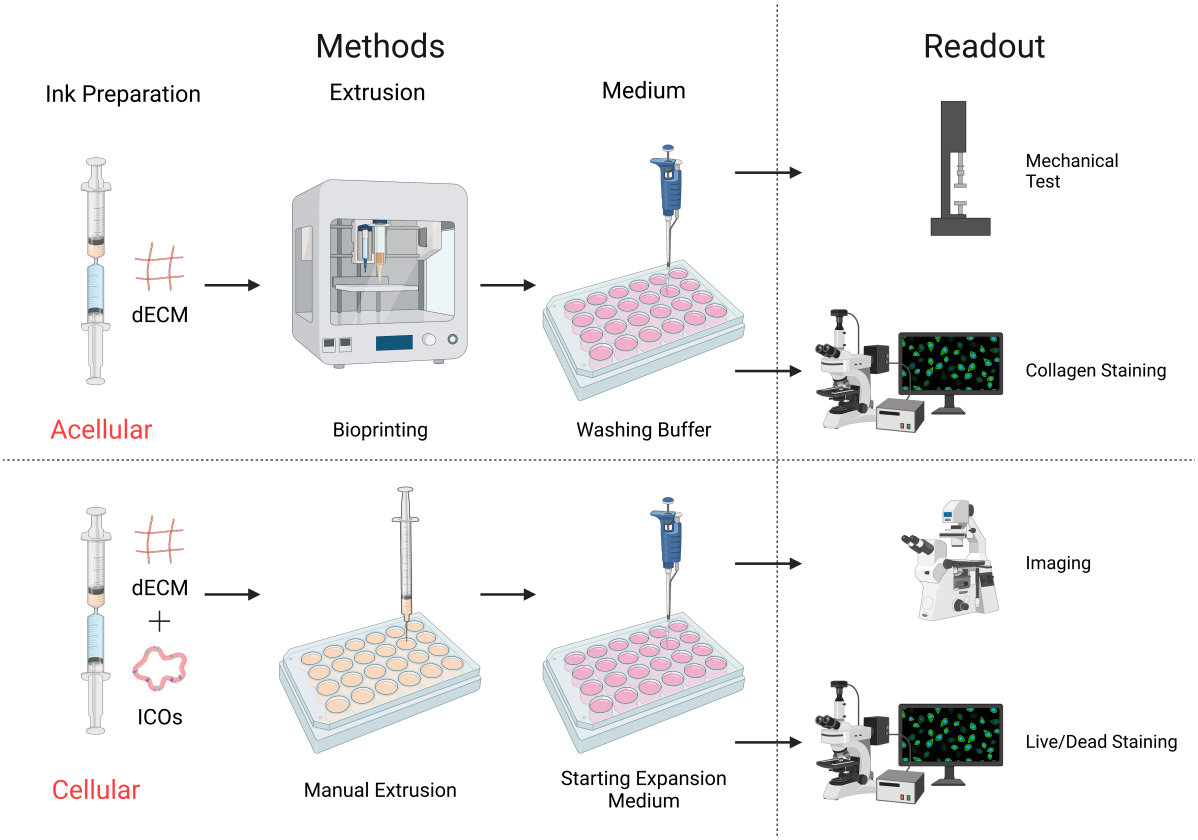

Figure 2.10: Graphical illustration of the methodologies employed in this project. The methodology included two types of experiments: acellular with bioprinting and cellular with manual extrusion. The readouts of each experiment are included

3

Results

In this section, the results obtained for developing a bioink composed of HAT, dECM, and liver organoids are presented. The first section includes the results associated with creating a 3D printable ink for an extrusion-based bioprinter. The second section describes the result for creating a bioink cytocompatible for liver organoids.

3.1. Formulation of a printable HAT and dECM ink

The optimisation of the ink composition, as well as the 2D and 3D shape fidelity post-printing, and the stiffness of the prints, are demonstrated. The focus in this first part was to develop a printable ink for an extrusion-based bioprinter.

3.1.1. Optimisation of ink composition for printability

The ink formulation was realised based on previous work [35, 38–40]. An iterative procedure was employed to create a printable ink.

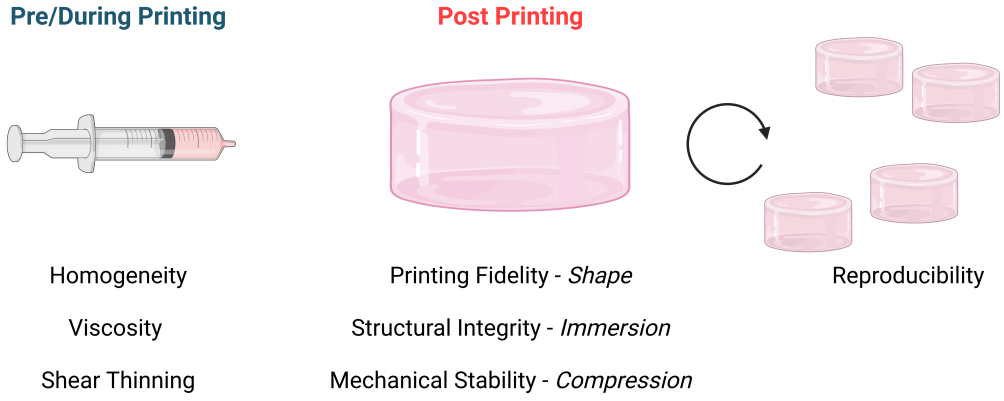

Figure 3.1: Graphical illustration of the requirements for a printable ink, with the test realised to evaluate each requirement

The requirements for the ink are shown in Fig.3.1. Before printing, the consistency of the ink had to be homogeneous. While printing, it had to have shear-thinning properties described by an ink that has little resistance under a high shear rate, when being extruded through the nozzle [3]. However, under a low shear rate after being deposited, it must recover and become more viscous to retain its structure. These shear-thinning properties reduce the amount of stress experienced by the cells during extrusion, thereby enhancing their viability.

Post-printing, the ink had to have shape fidelity, which meant that the printed scaffold should match the GCode design. The structural integrity of the scaffolds was assessed with an immersion test in AdvMEM/F12. The mechanical stability was evaluated by using compression tests on the day of the print and over three days. The last requirement was that the ink should produce reproducible prints, which should be achieved by employing the same methodology and material concentrations. In this way, the ink should possess similar shear-thinning properties, resulting in consistently printed scaffolds across multiple experiments.

To test the requirements previously mentioned, a testing procedure was followed. Firstly, the homogeneity of the ink was verified by manual extrusion on a glass slide. Once the homogeneity was confirmed, the ink was then printed using 2D GCode, seen in Fig.2.6. Lastly, if the ink exhibited shear-thinning properties it was 3D printed in a 24 well plate. The shear-thinning properties behaviour was determined by observing the viscosity of the ink during extrusion. The ink with high fluidity required low pressures (10-15 kPa) and high printing speeds ($>$ 35 mm.s^{-1}). In contrast, the viscous ink required higher extrusion pressures ($>$ 20 kPa) and lower printing speeds ($\backsim$ 30 mm.s^{-1}).

The ink was optimised by altering the concentrations of the components. Table 3.1 summarises the tested concentrations for each material. Concentrations suitable for printing are denoted in blue, whereas unsuitable ones are marked in red.

Table 3.1: Assessment table for the different concentrations of materials used to formulate a printable ink. In blue suitable concentrations and red unsuitable concentrations for 3D printing

Component	**Concentration**			
HAT	3 % w/v	5 % w/v		
H_2O_2	0.17 mM	0.51 mM	0.85 mM	
HRP	0.1 U.mL^{-1}	0.3 U.mL^{-1}	0.5 U.mL^{-1}	
dECM	0 mg.mL^{-1}	0.2 mg.mL^{-1}	0.6 mg.mL^{-1}	1.5 mg.mL^{-1}
EO Y	0 % v/v	0.01 % v/v	0.02 % v/v	

HAT Concentration

Two HAT concentrations were investigated: 3% and 5% w/v. For both concentrations, equal amounts of HRP, H_2O_2 and EO Y were added: 0.1 U.mL^{-1}, 0.51 mM and 0.01% v/v EO Y respectively. A full overview of the ink composition is found in Table 3.1. The inks were extruded using the same range of pressures, 19-25 kPa implying the inks were not too fluid (Fig.3.2). Both inks were over-extruded due to the low printing speed of 20 mm.s^{-1}, resulting in a higher quantity of material deposited. When comparing the inks, the 3% HAT had a lower viscosity than the 5% HAT. The line thickness of the 5% HAT was more consistent throughout the print, therefore we observe fewer variations between prints. This suggests that the 5% HAT ink was more printable than the 3% HAT.

H_2O_2 Concentration

Printability as a function of H_2O_2 concentration was investigated at three concentrations: 0.17, 0.51, and 0.85 mM. An upper boundary of 0.85 mM was chosen due to the cytotoxic effect of the H_2O_2 on organoids at high concentrations [43, 44]. The inks had equal amounts of HRP, EO Y, and HAT at 0.1 U.mL^{-1}, 0.01% v/v, and 5% w/v, respectively.

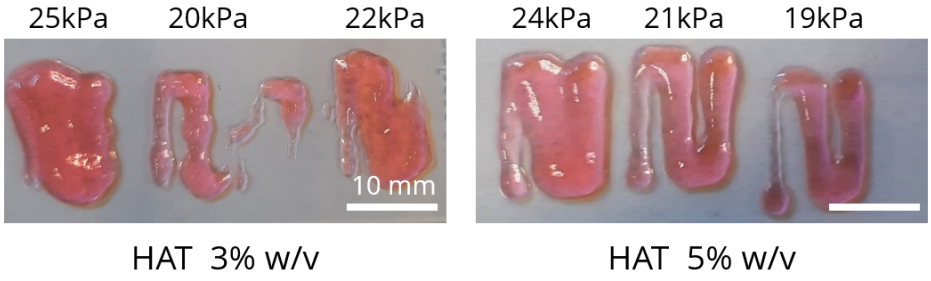

Figure 3.2: Printed 2D lines, with a 22G nozzle. Effect of variation for 3% and 5% w/v HAT concentration. The print was repeated three times using different pressures. Scale Bars 10 mm

Cubic scaffolds were printed in 24 well plates cubes, as seen in Fig.3.3. The ink with 0.51 mM H_2O_2 is shown on the left and the 0.85 mM on the right. The 0.17 mM H_2O_2 concentration was not included. as it did not recover after extrusion. The printing speed was 25 mm.s^{-1} for the 0.51 mM and 0.85 mM inks. The 0.85 mM ink required a higher extrusion pressure (23 kPa) as it was more viscous than the 0.51 mM ink (18-20 kPa).

Hence, from the top view the 0.51 mM H_2O_2 ink was printable into a cubic scaffold, however, it was less controllable and the reproducibility from one well to another was lower than the 0.85 mM H_2O_2. From the side view, the top of the scaffolds was not perfectly flat. A dome geometry was observed instead of a cubic shape. The 0.51 mM and 0.85 mM ink were promising as they were the only inks that could be printed in 3D.

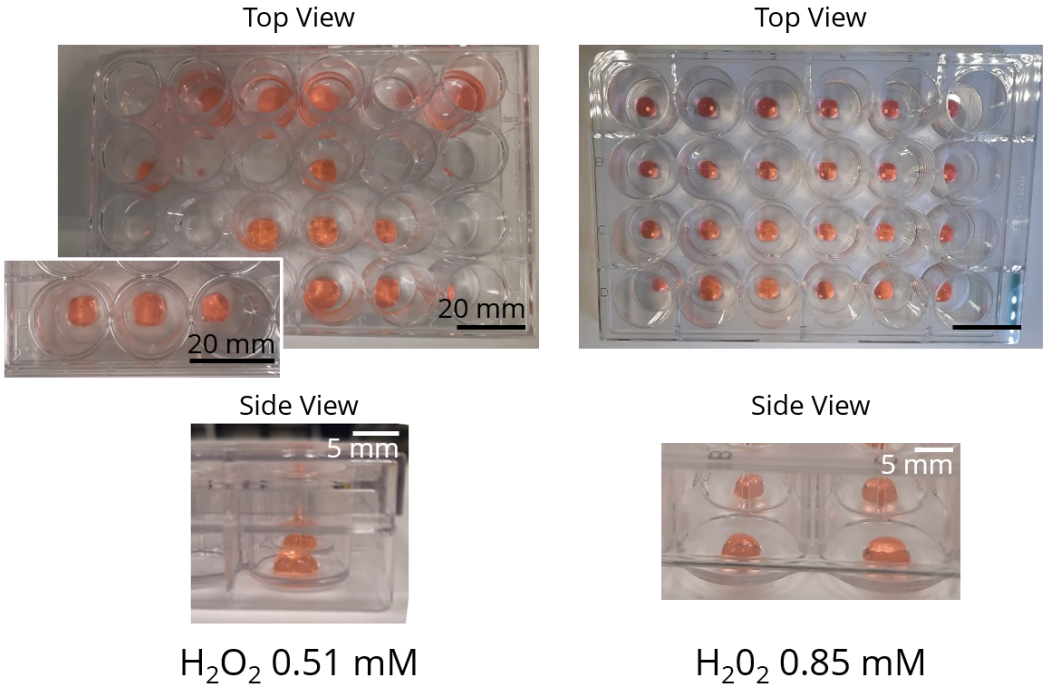

Figure 3.3: Effect of variation of the H_2O_2 concentration. Three layers were printed using a 3D GCode in a 24 well plate, with a 22G nozzle. Scale Bars: top view 20 mm, side view 5 mm

HRP Concentration

The effect of HRP concentration was investigated, as the enzyme triggers the enzymatic reaction converting the fluid ink into a gel-like material [45]. Three 5% w/v HAT inks were prepared with 0.1, 0.3, or 0.5 U.mL^{-1} of HRP. The H_2O_2 concentration was fixed to 0.85 mM and the EO Y at 0.01% v/v. The

inks were manually extruded, therefore information on speed and pressure could not be provided. The most continuous line with the smallest variation in thickness was achieved with the ink with the lowest HRP concentration, as shown in Fig.3.4. As HRP concentrations increased, the lines became less defined, indicating a less homogeneous ink that dissociated. Normally, an increase in HRP decreases the gelation time, indicating a more crosslinked ink [37]. However, these results suggest that there is a limit to the HRP concentration at which an inverse reaction occurs. The HRP concentration selected was 0.1 U.mL^{-1} based on these results.

Figure 3.4: Effect of variation of the HRP concentration. Manual extrusion on a glass slide using a 22G nozzle. Scale Bars 10 mm

dECM Concentration

The influence of dECM concentration was examined by using three concentrations of dECM at 0.2, 0.6, and 1.5 mg.mL^{-1} along with a control print, while keeping fixed the concentrations of HAT, HRP, and EO Y at 5% w/v, 0.1 U.mL^{-1}, and 0.01% v/v, respectively. In the control well plate, without dECM, the entire 24 well plate was printed at a pressure of 23 kPa and speed of 25 mm.s^{-1}. Twenty-two, twenty, and nine scaffolds were printed with the 0.2, 0.6, and 1.5 mg.mL^{-1} dECM concentration, respectively, as seen in Fig.3.5. The 0.2 mg.mL^{-1} ink was printed at an extrusion pressure of 28-35 kPa and speed of 27 mm.s^{-1}, while the ink with 0.6 mg.ml^{-1} was printed at higher pressures of 30-40 kPa and a lower printing speed 25 mm.s^{-1}. Finally, the 1.5 mg.ml^{-1} ink was printed with the highest pressures of 32-45 kPa at 20 mm.s^{-1}.

These results imply that higher concentrations of dECM result in more viscous ink, harder to extrude. Consequently, higher extrusion pressures and lower printing speeds were selected. Moreover, the increase in dECM concentration resulted in a gradual increase of pressure to maintain a consistent extrusion for each well, indicating that the dECM was gelating over time. This observation suggests a rise in the temperature of the ink since the gelation process is temperature dependent. The inks without dECM and 0.2 mg.mL^{-1} dECM were explored more extensively.

EO Y Concentration

Another parameter explored was the concentration of the photo-crosslinker Eosin Y. Eosin Y was chosen over lithium phenyl-2,4,6-trimethylbenzoylphosphinate (LAP) or irgacure photoinitiators as it uses visible green light ($\backsim$ 510 nm) for curing which is more cytocompatible than UV light (0-400 nm) [46].

Two inks were prepared with a concentration of 0.01% and 0.02% v/v EO Y and 5% w/v HAT, 0.85 mM H_2O_2, 0.1 U.mL^{-1} HRP. The 0.02% v/v EO Y ink reacted with the ambient light resulting in an ink photo-crosslinked prior to being extruded, hence it was not further investigated. To avoid photo-crosslinking before bioprinting a nozzle protector was designed to obstruct any light on the nozzle tip (Section 2.8).

Structural Integrity

The structural integrity was evaluated by the immersion of the scaffolds in AdvDMEM/F12 for three days. The scaffolds that were printed with 5% w/v HAT, 0.51 and 0.85 mM H_2O_2, 0.1 U.mL^{-1}, 0 and 0.2 mg.mL^{-1} dECM and EO Y remained intact, suggesting that they could provide a suitable 3D environment for the ICOs to grow, for three days.

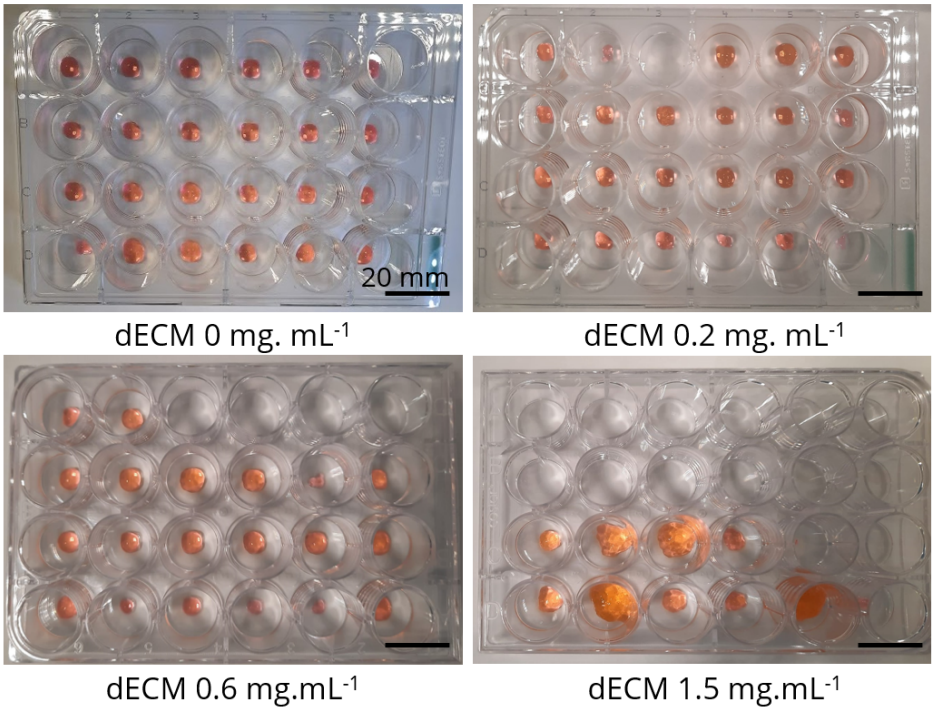

Figure 3.5: Effect of variation of the dECM concentration. Three layers were printed using a 3D GCode in a 24 well plate, with a 22G nozzle. Scale Bars 20 mm

To conclude the 5% w/v HAT ink with 0.1 U.mL^{-1} HRP and two concentrations of H_2O_2 were selected. Even if the 0.51 mM H_2O_2 had poor printability and reproducibility, it was selected for evaluating the effect of hydrogen peroxide on the organoids. In addition, an analysis was conducted to evaluate the comparative stiffness and cytocompatibility between one ink containing dECM and the other lacking dECM. The ink with the lowest dECM concentration of 0.2 mg.mL^{-1} was chosen over the 0.6 mg.mL^{-1} due to its consistent extrusion pressure and reproducibility. Table 3.2 gives the abbreviation used for the four inks hereafter in the project.

Table 3.2: Table with the abbreviation used throughout the report for the ink preparation

	Material Concentration		
Abbreviation	**HAT (% w/v)**	**H_2O_2 (mM)**	**dECM (mg.mL^{-1})**
0.51 HAT	5	0.51	0
0.51 dECM	5	0.51	0.2
0.85 HAT	5	0.85	0
0.85 dECM	5	0.85	0.2

3.1.2. 2D Shape Fidelity

In the previous section, four inks were formulated and selected for their capacity to be bioprinted. These inks included 0.51 HAT, 0.51 dECM, 0.85 HAT, and 0.85 dECM (Table 3.2). Shape fidelity served as an assessment method for evaluating the quality of the printed scaffolds, by calculating the resemblance of the print to the original GCode. The most printable ink was selected based on its ability to achieve the highest level of similarity to the GCode.

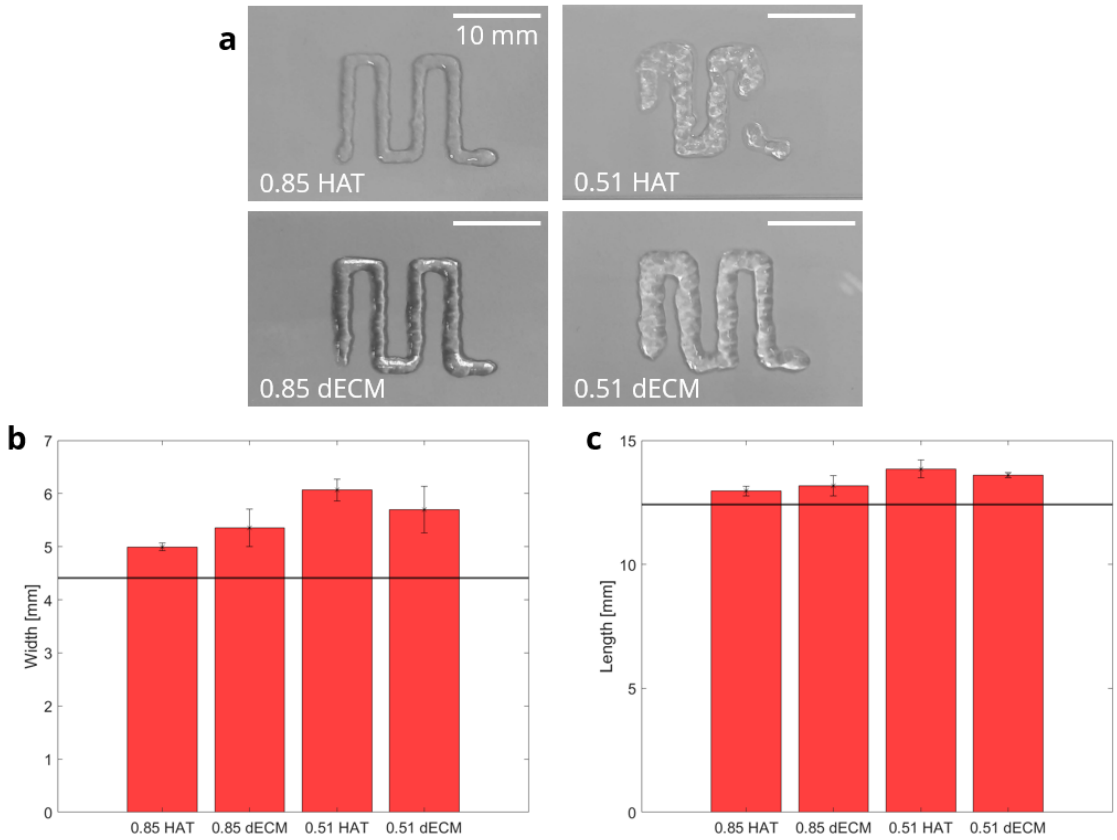

Figure 3.6: 2D Shape Fidelity of four inks. a. Image of the four inks printed on a glass slide. Scale Bars 10 mm, b. Bar plots of the measured width [mm] of the 2D lines for each ink printed with the deviation from the original GCode (horizontal black line), (n=3), c. Bar plots of the measured length [mm] of the 2D lines for each ink printed with the deviation from the original GCode (horizontal black line), (n=3)

The four inks were printed using the 2D GCode described in Section 2.2.4 are shown in Fig.3.6.a. The 0.85 HAT was printed at a pressure of 22 kPa and a speed of 25 mm.s^{-1}, while the 0.85 dECM had a pressure of 32 kPa and printing speed of 25 mm.s^{-1}. In comparison, the 0.51 mM inks both used an extrusion pressure of 17 kPa, and had different printing speeds, with the 0.51 HAT printed at 28 mm.s^{-1} and the 0.51 dECM printed at 20 mm.s^{-1}. These results imply that the 0.85 mM inks were more viscous than the 0.51 mM inks. Additionally, the addition of dECM increased the extrusion pressure or decreased the printing speed, indicating that the ink was harder to extrude and less fluid. Therefore, the 0.85 mM inks were more homogeneous resulting in a more constant deposition and smaller line thickness than the 0.51 inks (Fig.3.6.a). The measured width of the inks validates that the 0.51 inks were over-extruded and even discontinuous Fig.3.6.a & b. In contrast, the 0.85 inks were closer to the original design than the 0.51 inks, Fig.3.6.b & c.

The shape fidelity [%] was based on the percent error of the length and width of the printed line as defined in Section 2.2.5 and depicted in Fig.3.7. The bars closer to 100% indicate a higher resemblance of the printed scaffolds to the original GCode.

The shape fidelity analysis revealed that the 0.85 HAT and 0.85 dECM inks had higher shape fidelity for both the length and the width, with values of 95.6% and 93.9%, and 86.7% and 78.6%, respectively.

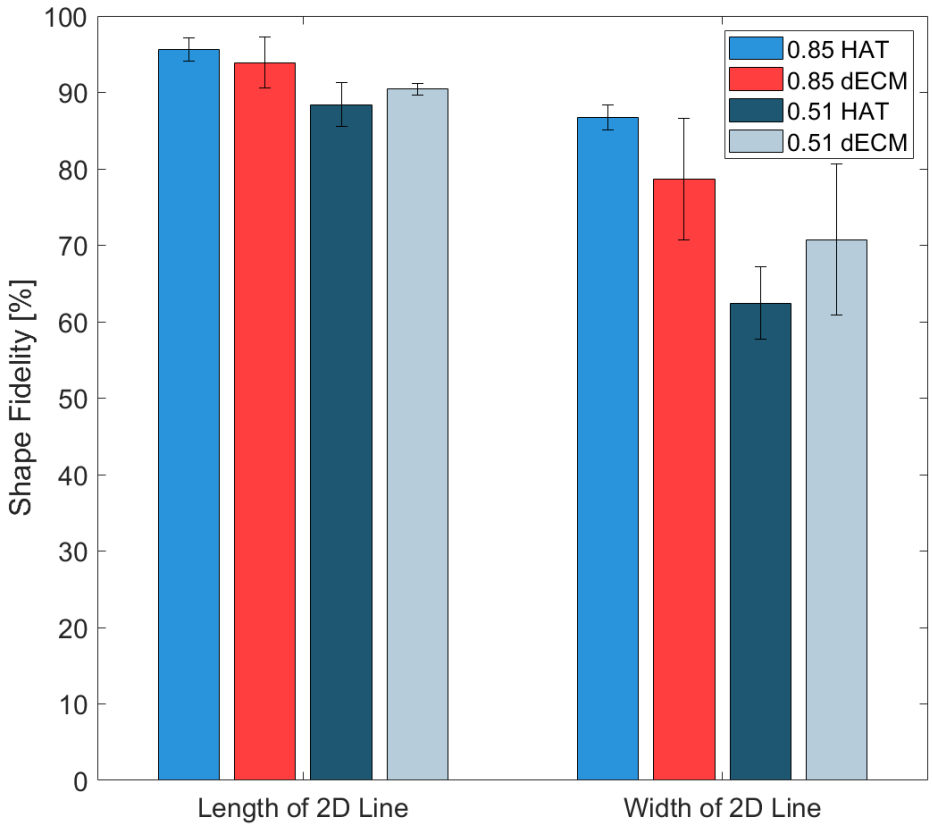

Figure 3.7: Bar plots illustrating the shape fidelity in % of the prints for the length and width of the printed lines for each ink (n=4)

On the other hand, the 0.51 HAT and 0.51 dECM inks had lower shape fidelity for the length and width, with values of 88.4% and 90.4%, and 62.4% and 70.7%, respectively. The average shape fidelity for the length was 92.1%, in comparison to 74.6% for the width. The difference in shape fidelity between the length and width can be explained by the toolpath, which resulted in less stretching of the ink in the length direction.

Although the addition of dECM did not have a clear impact on the shape fidelity of the inks, the 0.85 HAT ink showed a higher shape fidelity than the 0.85 dECM ink. Conversely, the inverse was observed for the 0.51 HAT and 0.51 dECM ink. These results can be explained by the limited shelf-life of the H_2O_2 used for the experiments.

Based on the shape fidelity results, the 0.85 inks, more specifically the 0.85 HAT ink were found to be the most suitable for printing 2D lines.

3.1.3. 3D Shape Fidelity

Similarly to the previous section, the shape fidelity was calculated for the base area and height of 3D printed scaffolds, in contrast to the length and width as investigated in the previous section.

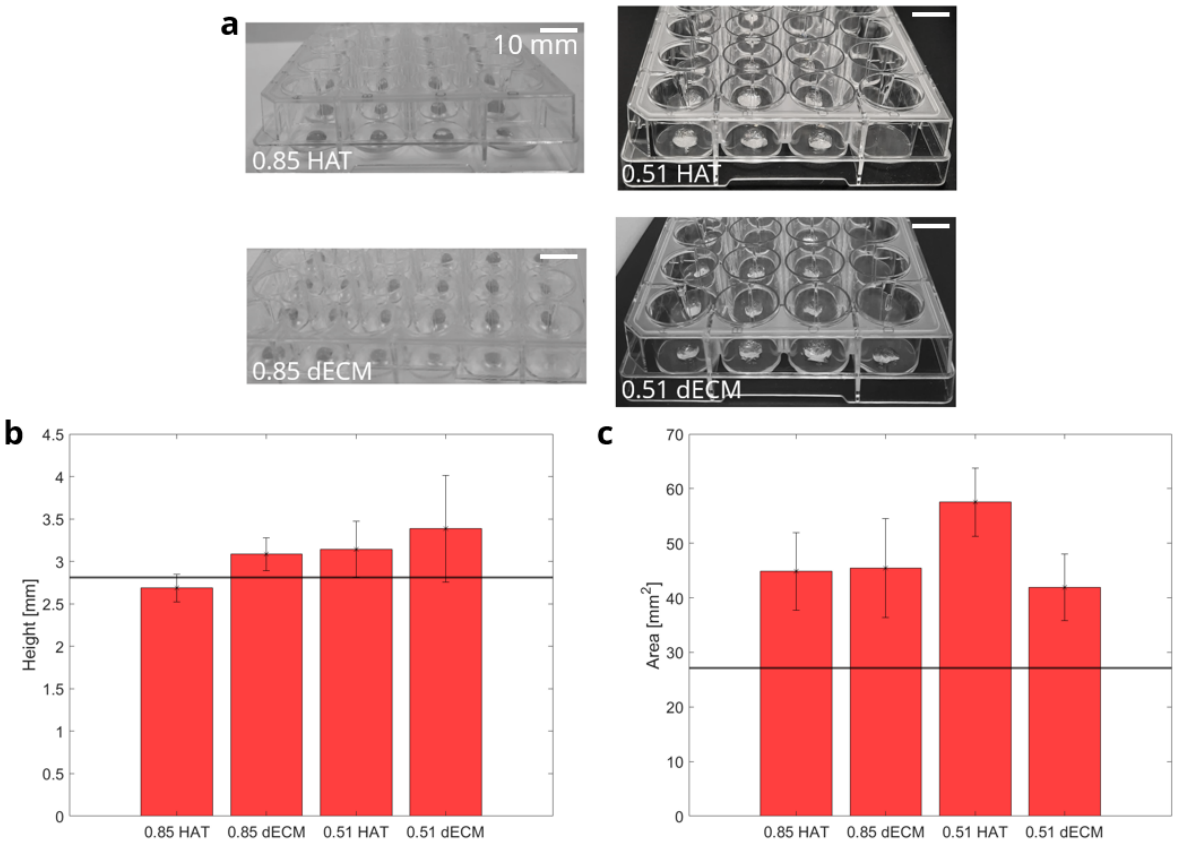

Figure 3.8: 3D Shape Fidelity of four inks. a. Image of the four inks printed in 24 well plates. Scale Bars 10 mm, b. Bar plots of the measured height [mm] of the 3D scaffold for each ink printed with the deviation from the original GCode (horizontal black line), (n=4), c. Bar plots of the measured area of the 3D scaffolds for each ink printed with the deviation from the original [mm^2] GCode (horizontal black line), (n=4)

The four inks printed using the 3D GCode described in 2.2.4 are shown in Fig.3.8.a. The bioprinter printed from one well to another, until the cartridge was empty. The 0.85 HAT ink and 0.85 dECM inks were printed at a speed of 25 $mm.s^{-1}$ and 27 $mm.s^{-1}$, respectively. The pressure of the 0.85 HAT ink was 23 kPa, whereas the pressure of the 0.85 dECM was altered from 28-35 kPa during printing. However, the 0.51 HAT ink was printed at a pressure of 18 kPa as opposed to 28kPa for the 0.51 dECM. The printing speed of the 0.51 HAT and 0.51 dECM was 28 $mm.s^{-1}$ and 23 $mm.s^{-1}$, respectively.

The consistency of the inks was homogeneous, and the scaffolds were consistently printed well to well (Fig.3.8.a). The scaffolds with 0.51 mM H_2O_2 appeared bigger than the 0.85 inks, due to over-extrusion. Consequently, the well plates were not fully printed, when employing the inks with the smallest concentrations of H_2O_2. Furthermore, the height and area of the scaffolds were taller and wider than the reference GCode value, except for the height of the 0.85 HAT, which was shorter Fig.3.8.b. & c. During the bioprinting process, all the inks were over-extruded.

The shape fidelity [%] was evaluated by calculating the percent error of the height and area of the 3D printed scaffolds compared to the reference GCode as illustrated in Fig.3.9. The shape fidelity of the 0.85 HAT and 0.85 dECM, in terms of height, was 95.6% and 90.2%, respectively. The 0.51 HAT and 0.51 dECM had lower values of 88.3% and 79.5%, respectively. The shape fidelity of the area was 34.8%, 32.6%, 11.9%, and 45.7% for 0.85 HAT, 0.85 dECM, 0.51 HAT, and 0.51 dECM, respectively.

The fidelity of the printed height was generally higher than the area for all inks. The average shape fidelity of the printed height for all the prints was 88.4%, in comparison to 31.2% for the area. However,

the area of 0.51 HAT showed a very low area-shape fidelity of 11.9%, which accounted for the lower overall area fidelity.

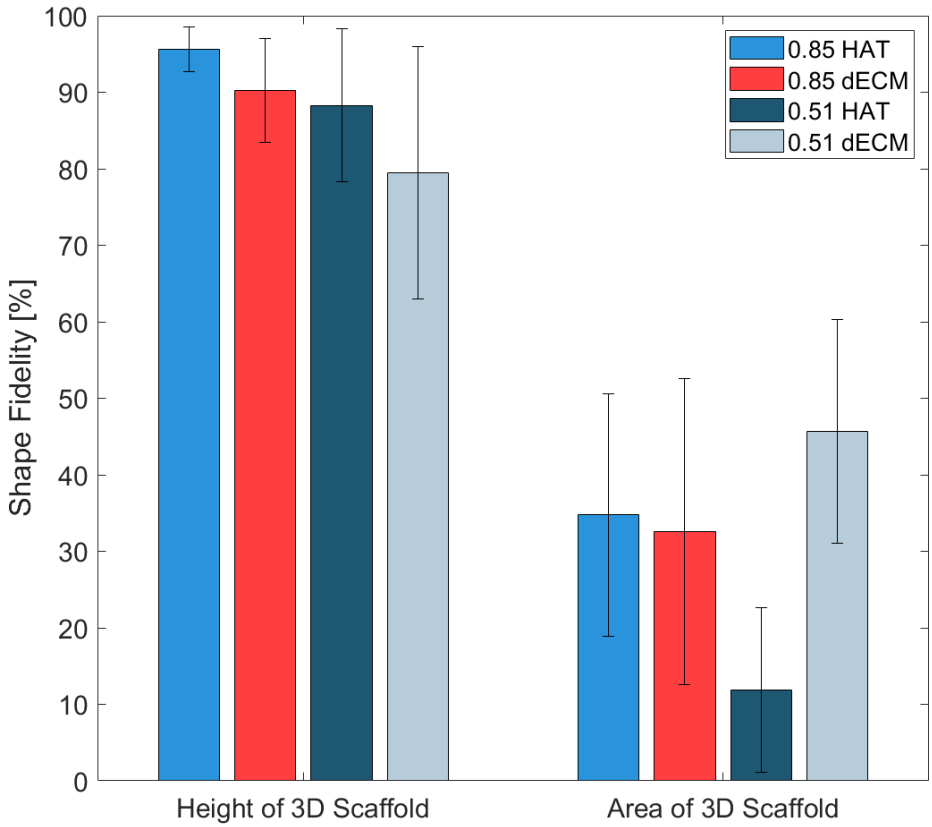

Figure 3.9: Bar plots illustrating the shape fidelity in % of the prints for the height and area of the 3D scaffold for each ink (n=4)

The GCode includes some pores however all the printed scaffolds were filled with ink and no pore were present. The resulting 3D scaffolds had a dome shape and were not cubic (Fig.3.10).

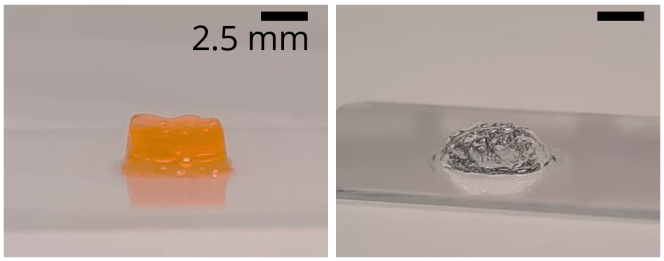

Figure 3.10: Side view of two printed scaffolds using the same GCode (Fig.2.7). The left scaffold was printed on a glass slide using commercial ink (CellStarter, CellInk, BIO X), while the right was printed using 0.51 HAT ink. Scale Bars 2.5 mm

The 2D and 3D shape fidelity (Section 3.1.2 & 3.1.3) demonstrated that the inks were over-extruded in comparison to the GCode. The 2D shape fidelity was found to be closer to the original design compared to the 3D shape fidelity, especially due to the low fidelity of the printed scaffold's area.

To conclude, the 2D and 3D shape fidelity showed that the 0.85 HAT and the 0.85 dECM were the closest inks to the original GCode design.

3.1.4. Stiffness of scaffolds printed with 0.85 HAT, dECM inks & 0.51 HAT, dECM inks

Compression tests were realised to evaluate whether the printed scaffolds were in the range of healthy liver stiffness (1.2-6.0 kPa) [5, 6, 47]. The Young's Modulus was determined from the compression tests, described in Section 2.2.8. On the day of printing, compression tests were performed on four scaffolds (n=4) printed for each ink defined in Table 3.2.

The mean and error bars (STD) of the Young's modulus for the four inks are represented in Fig.3.11. The printed scaffolds with the 0.85 dECM ink had a stiffness of 2.91 $\pm$ 0.64 kPa, while those printed with 0.85 mM HAT ink had a stiffness of 1.64 $\pm$ 0.34 kPa. Scaffolds printed had a stiffness of 3.92 $\pm$ 1.25 kPa and 1.41 $\pm$ 0.59 kPa for the 0.51 dECM and 0.51 HAT, respectively. There was a significant difference among the four different inks, as the *p < 0.05.

The dECM scaffolds had a greater stiffness with an average of 3.40 $\pm$ 1.01 kPa than the scaffolds only composed of HAT, which had an average of 1.52 $\pm$ 0.46 kPa. There was a significant difference between the HAT and dECM scaffolds, where *p < 0.05. The 0.51 dECM ink had a greater stiffness than the 0.85 dECM ink (3.88 $\pm$ 1.38 kPa and 2.91 $\pm$ 0.64 kPa, respectively), whereas the 0.85 HAT was stiffer than the 0.51 HAT ink. Therefore, there was no statistically significant difference between the different H_2O_2 concentrations.

To conclude, the scaffolds containing dECM had a greater stiffness than the scaffolds without dECM. The concentration of H_2O_2 may have an impact on the stiffness of the scaffolds, but the results were not statistically significant. All of the printed scaffolds were in the same range as the stiffness of healthy liver.

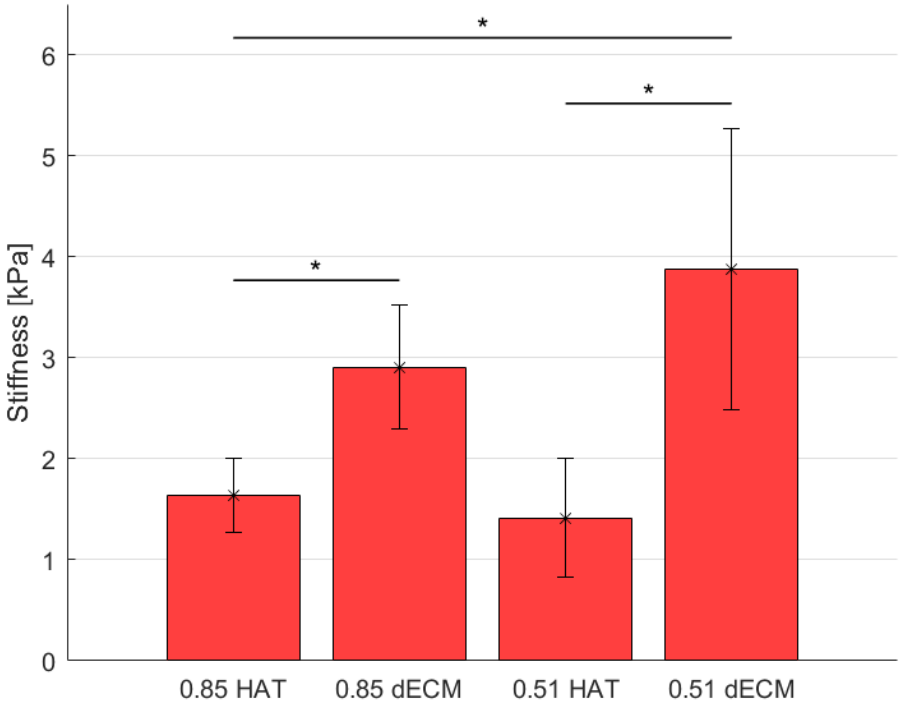

Figure 3.11: Bar plot of the evaluated the Young's modulus for the 0.85 HAT, 0.85 dECM, 051 HAT, and 0.51 dECM scaffolds, on the day of printing. The error bars represent the mean of the stiffness calculated for four scaffolds and its associated error as the standard deviation, (n=4), *:p $\leq$ 0.05

3.2. Formulation of a cytocompatible bioink for ICOs

The previous section described the optimisation of the ink composition to meet the criteria illustrated in Fig.3.1. The selection of four inks, namely 0.85 HAT, 0.85 dECM, 0.51 HAT, and 0.51 dECM was based on their printing fidelity, structural integrity, mechanical stability, and reproducibility.

The second challenge for bioinks developed for extrusion-based bioprinting was the evaluation of cytocompatibility. The objective of this section was to assess the viability of human donor-derived liver organoids in the previously formulated inks, more specifically the 0.85 HAT and 0.85 dECM inks that exhibited the best printability. The results associated with the incorporation of ICOs are presented in this section.

3.2.1. Influence of bioink composition on ICOs viability

To determine the viability of the ICOs in the ink, they were incorporated following Protocol 2.2.2. The ICOs were mixed with the 0.85 HAT and 0.85 dECM ink, along with 0.01% v/v EO Y. The first, second, and third rows of Fig.3.12 show the ICOs incorporated in BME (control), 0.85 HAT, and 0.85 dECM ink, after one and two days, respectively. From day 1 to day 2, the ICOs in the 0.85 HAT and 0.85 dECM have not grown or proliferated, while those in the BME showed growth. Furthermore, air bubbles and a pink stain from the EO Y were distinguishable in the inks. Within a day, the air bubbles vanished or were reduced in size, and the EO Y faded out of the scaffold.

The ICOs were non-viable in both bioinks 0.85 HAT and 0.85 dECM. The cause of the cell death was investigated to reformulate a bioink that would be viable for ICOs. The cell death could be attributed to the ink components which could be cytotoxic, such as a high concentration of H_2O_2 inducing cell death [48].

The effect of H_2O_2 concentrations and the reaction between H_2O_2 and HRP was further investigated and described in Appendix C. ICOs were plated in BME, an environment favourable for their growth and proliferation. In one experiment, expansion medium was mixed with a range of H_2O_2 concentrations (0.17, 0.51, 0.85 mM) and added to the wells. To simulate the ink formulation, a second experiment was conducted with the addition of HRP (0.1 $U.mL^{-1}$) and a range of H_2O_2 concentrations (0.17, 0.51, 0.85 mM) were mixed and left in the incubator for 30 min. From the experiments a concentration of 0.85 mM H_2O_2 was cytotoxic for the ICOs, hence the 0.85 HAT and 0.85 dECM inks were not further investigated.

In order to formulate bioinks that were viable for ICOs, lower H_2O_2 concentrations were explored based on the results described in Appendix C. Four dECM 0.2 $mg.mL^{-1}$ inks were made with a 0.34 mM or 0.51 mM H_2O_2 concentration, with or without the presence of EO Y (Fig.3.13). Low densities of ICOs are observed in the inks. A small number of alive ICOs were visible on day 1 in the 0.34 and 0.51 mM H_2O_2 inks. When EO Y 0.01% v/v was incorporated and photo-crosslinked under green visible light, ICOs did not survive. The effect of EO Y on ICOs in the 0.51 dECM ink was investigated and described in Appendix D. The experiment indicated that EO Y was another cytotoxic component of the ink. The results were validated by a Live/Dead staining on day 3. Thus, EO Y was removed from the ink composition to the detriment of structural integrity.

The 0.51 dECM was the only ink that did not dissolve two days after the incorporation of ICOs. In the 0.51 dECM ink, the ICOs were monitored for an additional two days. On day 1, many air bubbles were distinguishable in the ink (Fig.3.14), similarly to the previous experiments, they vanished from the ink. Small densities of ICOs were incorporated in the ink, where sample 3 had the most ICOs. The arrows from the microscope images point to some viable/dead ICOs. The growth and proliferation of the ICOs over three days were extremely weak or non-existent in the 0.51 dECM ink, in comparison to ICOs encapsulated in BME (Fig.B.1).

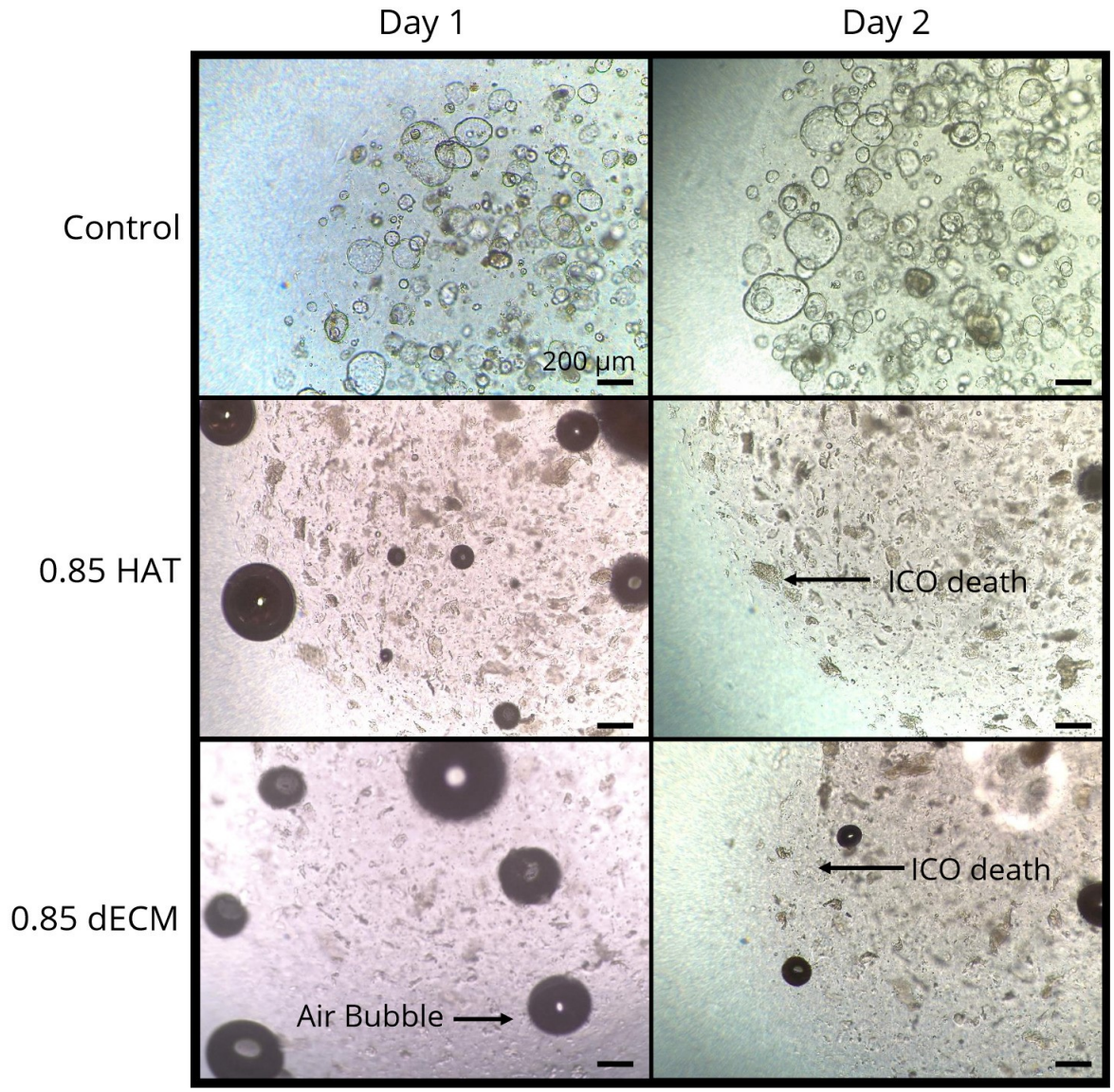

Figure 3.12: ICOs incorporated in BME, 0.85 HAT with EO Y, and 0.85 dECM WITH EO Y ink, after day 1 and day 2. Scale Bars 200 µm

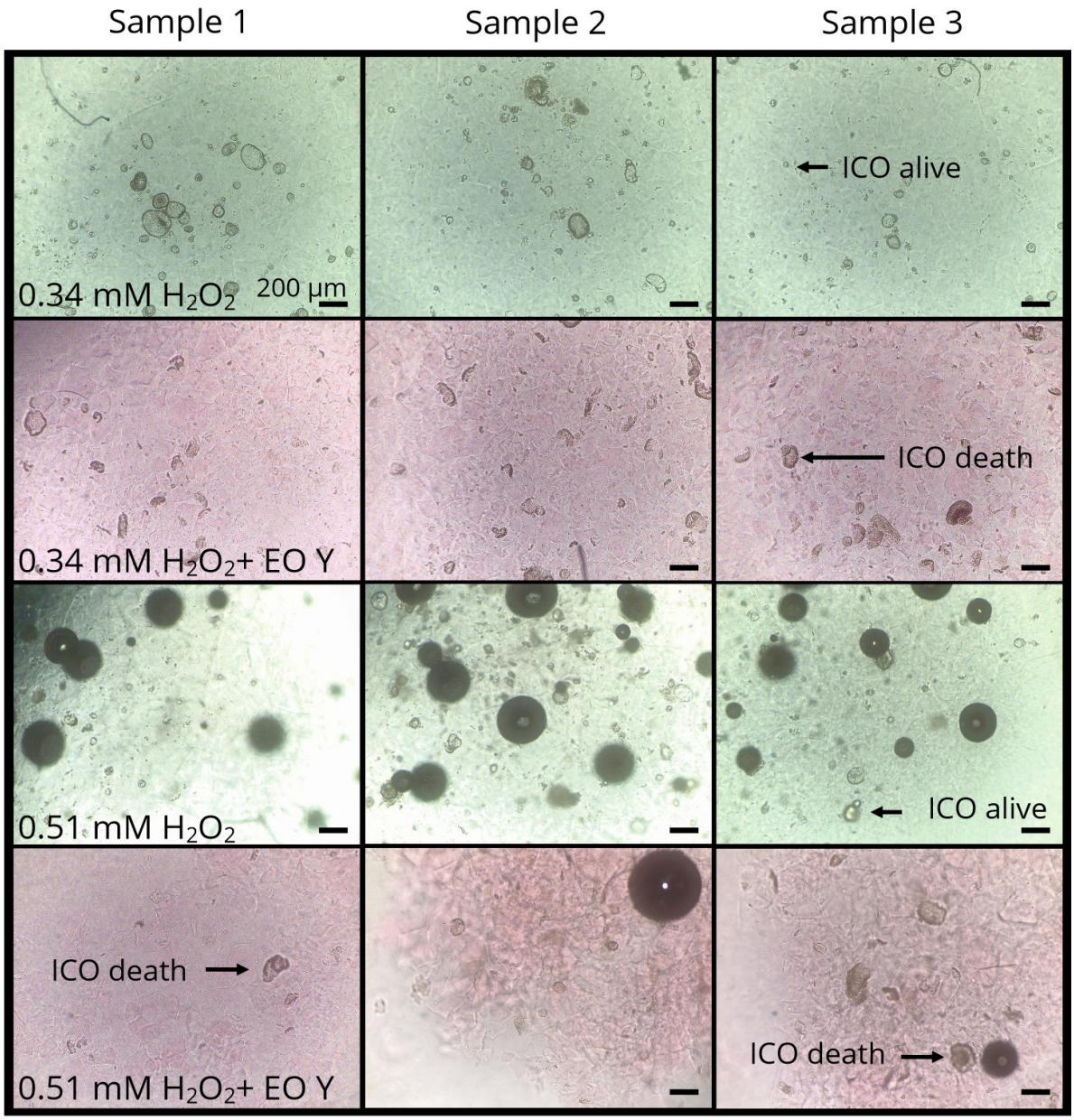

Figure 3.13: ICOs incorporated in four inks with 0.2 mg.mL^{-1} dECM with/without EO Y on the day after splitting. Scale Bars 200 µm

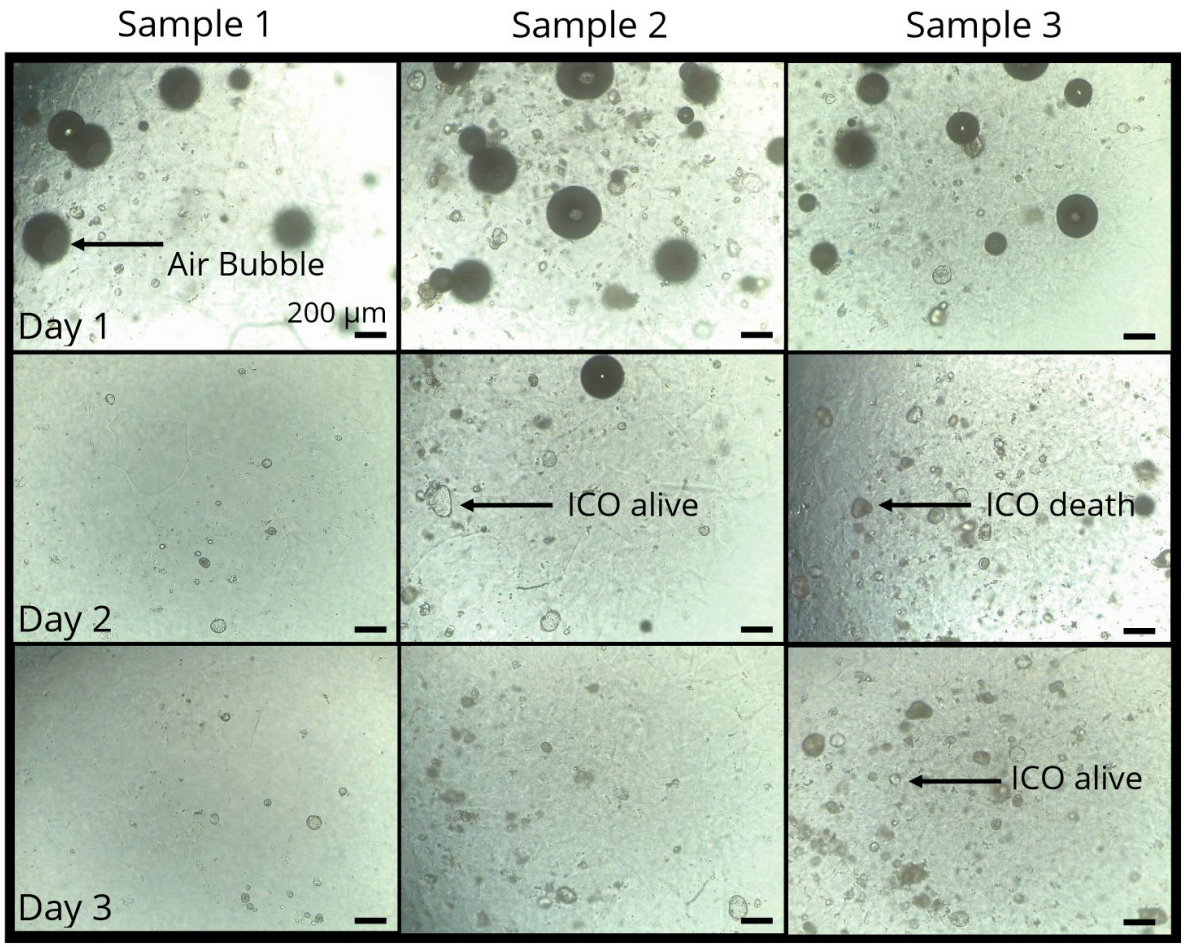

Figure 3.14: ICOs incorporated in the 0.51 dECM ink without EO Y, imaged on day 1, day 2, and day 3. Scale Bars 200 µm

ICO viability in the 0.51 dECM ink was determined through a Live/Dead staining. Alive ICOs are visible in Fig.3.15.a, labeled in green by the Live/Dead staining. To validate the findings, the experiment was replicated and the results were consistent, as shown in Fig.3.15.b. These results demonstrate that the bioink was cytocompatible for the ICOs.

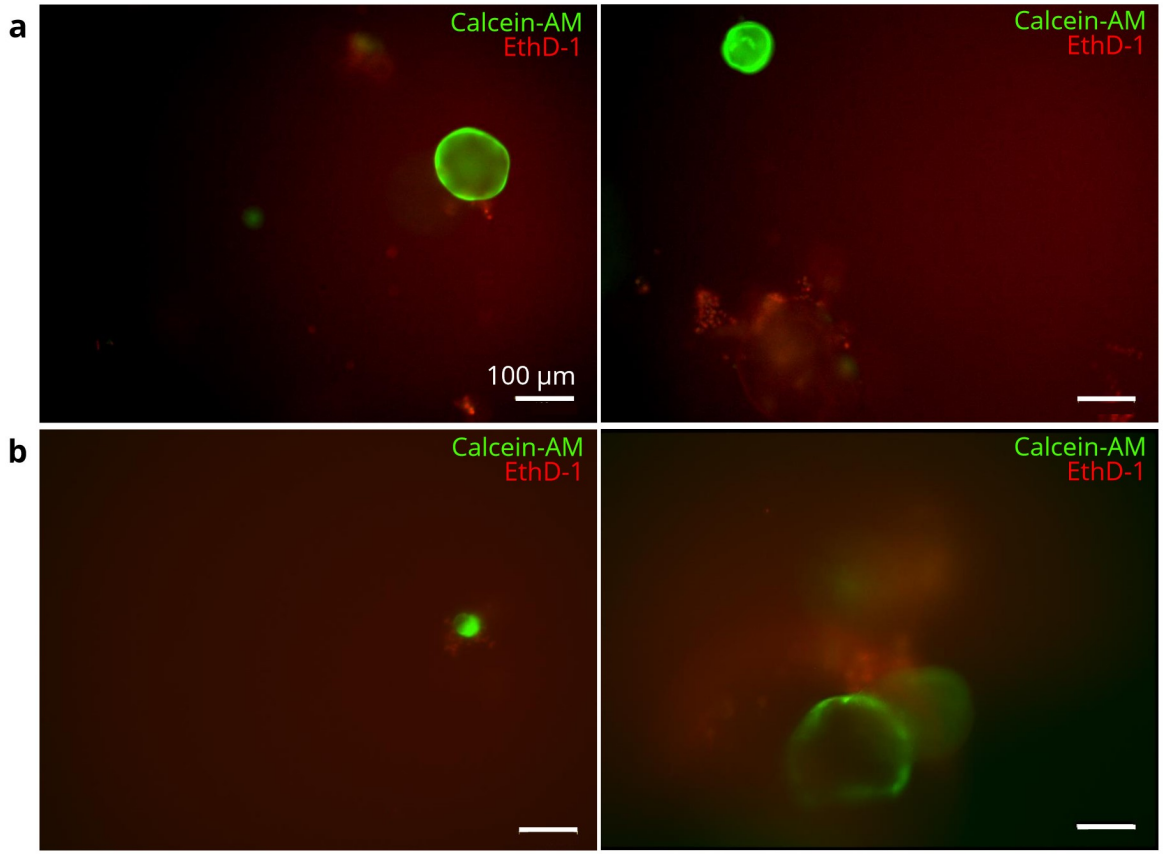

Figure 3.15: Live/Dead Staining on ICOs incorporated in the 0.51 dECM ink without EO Y. a. First experiment, b. Second experiment. Scale Bars 100 µm

3.2.2. Stiffness over 3 days of scaffolds printed with 0.51 dECM ink

To evaluate the mechanical properties of the printed scaffolds, a compression test was conducted on the 0.51 dECM ink, which was the only ink suitable for ICOs. The compression tests were carried out on three consecutive days. The duration for which ICOs were kept alive in the bioink. The compression was performed on the day of printing and the two subsequent days. The 0.51 dECM ink was prepared without incorporating ICOs and without EO Y. The Young's modulus was obtained using the methodology described in Section 2.2.8.

The same four samples were compressed over three days. The mean and error (STD) of the Young's modulus are presented in Fig.3.16. On the day of printing, the 0.51 dECM ink had a stiffness of 3.80 $\pm$ 1.40 kPa. On the next day, the stiffness was 4.12 $\pm$ 1.14 kPa, and on the last testing day 3.18 $\pm$ 0.35 kPa. The printed scaffolds did not have any statistical significance in stiffness over a three-day period. The results suggest that the scaffolds had similar stiffness over three days, which is advantageous for the growth of ICOs, as the 3D environment in which they are cultured remains constant.

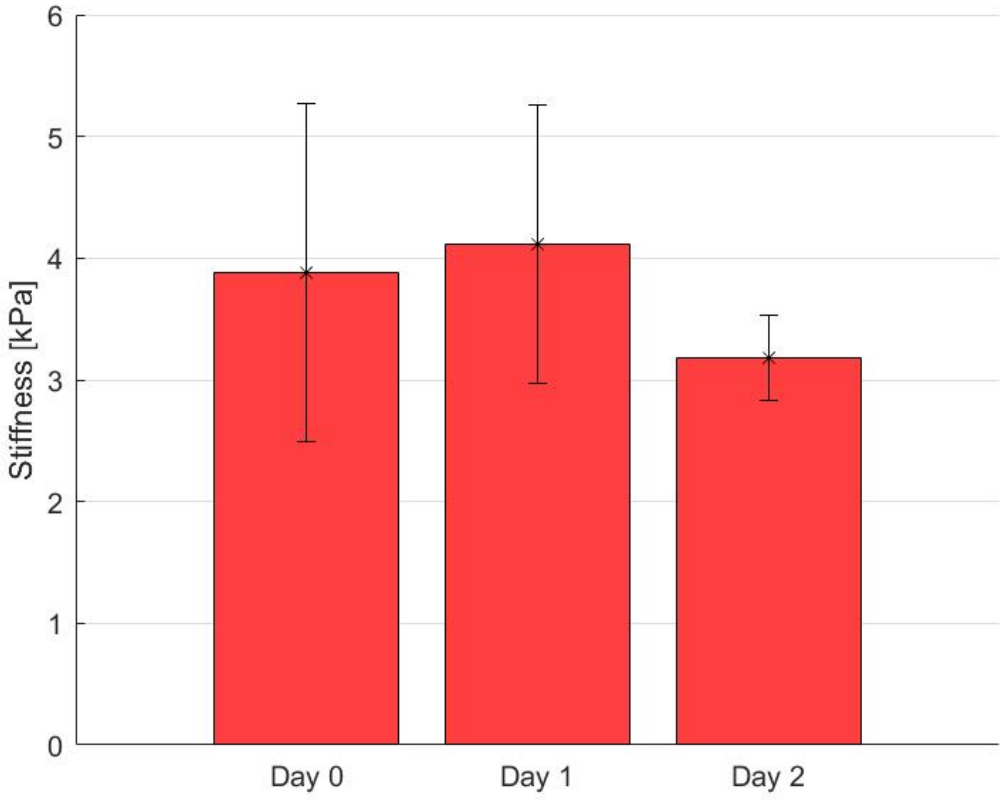

Figure 3.16: Bar plot of the evaluated the Young's modulus for the 0.51 dECM ink evaluated on day 0, day 1, and day 2. The error bars represent the mean of the stiffness calculated for four scaffolds and its associated error as the standard deviation, (n=4)

4

Discussion

The present study aimed to develop a cytocompatible bioink suitable for 3D bioprinting liver tissue. Initially, the ink composition was optimised for printability. Then, the ink's toxicity was evaluated on ICOs and the ink formulation was altered to obtain a viable bioink.

Several requirements needed to be fulfilled to formulate an ink with HAT, dECM, and organoids. One of the initial challenges was to achieve homogeneity and visible shear-thinning properties by optimising the concentrations of the components in the ink. By adjusting and fine-tuning the composition, four HAT inks with a concentration of 5% w/v were developed, two using 0.85 mM H_2O_2 and the other two using 0.51 mM H_2O_2. The 0.85 mM H_2O_2 inks showed better 2D and 3D shape fidelity.

The ink with 0.85 mM H_2O_2 was found to be more favourable as it resulted in an increased amount of crosslinking, leading to a more viscous ink. The results are coherent with prior research, which has shown that inks become more viscous for higher H_2O_2 concentration with fixed HAT [36, 37, 48]. Viscoelastic moduli were also found to increase with an increase of H_2O_2, indicating an increase in crosslinking [10]. Viscoelasticity is a measure that describes the capacity of a viscous ink to deform under external forces and return to its original form when the forces are removed due to its elastic properties.

H_2O_2 and HAT are interdependent materials, where an increase in the HAT concentration is translated by an increased amount of tyramine groups in the ink, resulting in a greater amount of potential crosslinks. Hence, by increasing the H_2O_2 concentration leads to a more entangled network of HAT groups, resulting in a denser polymer network. Nevertheless, the concentrations used in this study were higher than those reported in the literature, which employed 2.5-5 % w/v HAT and 0.17-0.7 mM H_2O_2. At higher concentrations, the research groups observed difficulties in extrusion, discontinuous prints, and potential cytotoxicity at higher concentrations [10, 37, 45].

In high concentrations, HA is a marker of fibrosis, therefore it may induce a fibrotic response from the cells when used at 5% w/v [49, 50]. Depending on the intended application of the bioprints the fibrotic response can be disadvantageous for healthy liver modeling, although it can be beneficial for generating liver disease models. Further investigations are necessary to determine the optimal concentration of HA for bioprinting applications.

Overall, the scaffolds had a low shape fidelity in comparison to other studies, resulting in a dome-shaped structure instead of the desired cubic shape [17, 20, 24]. This low shape fidelity can be attributed to several factors, including viscosity, shear-thinning, and swelling properties of the ink. Specifically, the viscosity which determines the ink's ability to flow is critical for achieving high printability. The ink must have a high viscosity and low shear rate [3]. The inks in this study were highly crosslinked, resulting in a viscous ink that was hard to extrude. The high viscosity induced surface tension along the nozzle and the ink, reducing the ink's ability to shear thin. Consequently, when printing the surface tension prevented the ink from accurately following the toolpath. Hence, the poor printability could be linked to the cubic design where the viscous and elastic ink did not follow the 90^o angles accurately and had a curved deposition seen by the dome-shaped scaffolds.

Multiple approaches could be employed to enhance the printing fidelity. One potential strategy is to develop an ink with a lower viscosity, which would facilitate the ink deposition process by reducing the friction between the ink and the nozzle. An equilibrium must be achieved in the development of an ink with desirable properties, specifically where the ink exhibits controlled flow characteristics with the production of a continuous filament rather than droplets. For example, this balance was disrupted when the HRP concentration exceeded 0.1 $U.mL^{-1}$.

The enzymatic crosslinking resulted in the formation of long polymeric chains with higher elasticity and shear rates. Another approach to improve the deposition and obtain a higher printability, the number of crosslinks must be reduced.

The selection of bioprinting equipment is a crucial factor that influences printing fidelity. For example, using a narrower nozzle can improve the precision of printing. However, in this study, a wider nozzle (22G) was preferred to ensure higher viability of ICOs by reducing the negative effects of shear forces resulting from higher extrusion pressures [51, 52]. Hence, to achieve higher printing fidelity, it is necessary to optimise the ink formulation further.

In the project, small amounts of liver dECM were incorporated into HAT inks. Small concentrations of dECM prevented the temperature-dependent gelation property of dECM to dominate the previously formulated HAT ink [53]. Compression tests showed a significant increase in scaffold stiffness in the presence of dECM compared to ink without dECM, indicating that the dECM was present in the scaffold post-printing. These findings are consistent with a previous study that observed an increase in stiffness when adding dECM to GelMA bioinks [17]. However, the presence and distribution of dECM in the scaffold could not be visualised through histology or immunofluorescence due to liver batch-to-batch variation or collagen loss from multiple freeze-thaw cycles. Freeze and slow thaw cycles were shown to denaturalise proteins [54, 55]. When formulating dECM bioinks, it is important to consider that the mechanical and biological outcomes may vary from batch-to-batch variation. Previous work mixed dECM usually derived from animals with conventional bioinks (GelMA, Alginate, gelatin) to develop printable and cytocompatible inks [9]. Nevertheless, these bioinks do not mimic the liver composition, are not immunogenically compatible, and lack direct clinical application. To date, this study is the first and only research using HAT and human dECM, which are two materials naturally present in the liver, to create a bioink suitable for EBB.

Compression tests were conducted to evaluate the stiffness of the liver scaffolds since research has indicated that cell response varies with stiffness [22, 47]. Specifically, a study found that primary hepatocytes in a 4.6 kPa dECM-HA gel over seven days demonstrated a decreased hepatocyte gene expression and cell stress. The optimal stiffness was 1.2-4.6 kPa for replicating *in vivo* response of primary hepatocytes [11]. The stiffness of the printed scaffolds ranged from 1.41 $\pm$ 0.59 kPa to 4.12 $\pm$ 1.14 kPa, consistent with the study's recommended range. These results suggest that the scaffold printed offer a favourable environment for the growth of primary hepatocyte, although liver organoids may respond differently. It was hypothesised that over time the stiffness would decrease, but no significant changes in stiffness were observed. The scaffolds fabricated in this study can provide a stable environment over three days for the ICOs. Additional work is needed for identifying concentrations of dECM and HA to replicate the biophysical and mechanical properties, equivalent to a healthy liver.

The second challenge of the project was to create a cytocompatible bioink. The ink with the most controllable extrusion and best shape fidelity was the 0.85 mM H_2O_2 inks, however, this ink was cytotoxic to the ICOs. The trade-off between printability and biocompatibility referred to as the biofabrication window was observed [3]. Hence, the potential cytotoxicity of the EO Y and H_2O_2 concentration were evaluated using ICOs in BME.

It was demonstrated that EO Y is cytotoxic only when exposed to visible light during the photocrosslinking step. The cell death could be attributed to the presence of free radicals that were not fully consumed after the reaction [56]. Free radicals can damage cell membranes, proteins, and DNA [57]. The printed scaffolds were exposed for 10 min (5 min from top + 5 min from bottom), as it was shown that this duration resulted in better shape preservation of the scaffolds than shorter exposition time [40]. Nevertheless, based on our findings to ensure ICOs viability the exposure time may need to

be reduced to the detriment of the structural integrity of the scaffolds [38]. Accordingly, to maintain the viability of ICOs, the photoinitiator was removed from the ink. As a consequence, the scaffolds lacked a secondary post-printing crosslinking step, which led to increased swelling and decreased printing fidelity. Another approach for preserving the shape of the scaffolds post-printing would be to substitute EO Y with ruthenium and sodium persulfate as a more cytocompatible photoinitiator for ICOs [58, 59].

Additionally, the effect of different H_2O_2 concentrations on ICOs in BME were inspected, as no comparable studies were published on ICOs with H_2O_2. The highest concentration of H_2O_2 affected the cells similarly to previous work done on other cell types [43, 44]. For instance, HUVECs were cultured in presence of 0.5 mM H_2O_2, their viability decreased to 50% in comparison to not having any H_2O_2 [43]. To assess the consumption of H_2O_2 during the HAT ink formulation, a separate experiment was conducted. Two constituents of the ink, H_2O_2 and HRP were mixed and incubated for 30 min, before supplementing the expansion medium to the ICOs in BME. Results suggest that the concentration of H_2O_2 decreased in the presence of HRP and EM, leading to a smaller impact on ICOs. While both experiments shed light on the effects of H_2O_2, they did not replicate the ICO encapsulation in the bioink. The organoids were in contact with the H_2O_2 in the dECM bioink, a lower concentration of 0.51 mM of H_2O_2 was chosen to limit the ICOs death. Furthermore, the ICOs were added at the final stage of the ink procedure to minimize the impact of the enzymatic reaction.

Liver organoids were alive for three days in a bioink made from human donor-derived dECM and ICOs. In the study, the ICOs viability was demonstrated, yet the growth and proliferation were not reported due to the limited amount of ICOs present in the final bioink. It is known that ICOs have a lower proliferation in liver dECM compared to BME [60]. BME is a mouse tumor-derived extract commercially available with a bioactive environment, stimulating cell proliferation, but unsuitable for clinical applications [60]. Consequently, the incorporation of liver dECM in bioinks could provide liver-specific biochemical cues that offer a superior approach for recapitulating the liver *in vivo* microenvironment in comparison to BME, for ICOs [60]. Other studies have reported similar findings when adding dECM to bioinks with different cell types, in which the mechanical, biophysical, and biochemical cues were inherited from the ECM, and led to an enhancement of cell function, cell viability, cell spreading, and hepatic differentiation of stem cells [16, 17].

As previously mentioned, the incorporation of small densities in the ink prevented the evaluation of the metabolic activity of ICOs using PrestoBlue. Future experiments should aim to contain larger cell densities to enable such evaluations. Additionally, the non-homogeneous distribution of the organoids in the ink highlights the need for a new protocol to ensure uniform mixing of the liver organoid pellet in the ink.

The ICOs were monitored for three days, however extending this time frame would allow a more comprehensive assessment of organoids' growth, proliferation, and viability. A longer culture duration would enable the evaluation of additional biological readouts for evaluating the presence of dECM. Furthermore, quantitative polymerase chain reaction (qPCR) could be used to examine the expression of liver-specific genes.

In this study, a bioink consisting of dECM, HAT, and incorporating ICOs was developed for prospective 3D bioprinting applications. 3D bioprinting offers several advantages in fabricating liver tissue, as a diverse range of parameters can be selected according to the application of the printed scaffold. However, the final prints lack the transport of nutrients and oxygen to organoids. As a result, researchers are investigating integrating organ-on-chip technology, microfluidic devices that incorporate perfusion systems with 3D bioprinting [61, 62]. The combination of these two technologies and the development of multi-organ-on-chips could be a promising approach to simulate the inter-organ communication aiming to mimic better the physiology and pathophysiology of the liver [63].

5

Conclusion & Recommendations

5.1. Conclusion

The aim of this thesis was to develop a bioink for liver 3D bioprinting applications. The novelty of the project resided in employing human donor-derived biomaterials from the liver such as dECM and organoids. The challenge of this project was to create a bioink with good printability and also providing a favourable environment for organoids to live.

Firstly, HAT and dECM inks were formulated to obtain a printable ink employing an extrusion-based bioprinter with a pressure-controlled extrusion-system. The inks were developed by tuning the concentrations of these materials. It was found that the 0.85 HAT and 0.85 dECM inks had the highest printability. These two inks had a high shape fidelity in 2D, with a resemblance in comparison to the original GCode. However, the 3D printability was lower. The scaffolds had a stiffness (1.41-4.12 kPa) in the range of a healthy liver (1.2-6.0 kPa), based on the compression tests.

The second objective was to incorporate liver organoids in this ink and investigate their viability over time. It was observed that in the ink previously formulated (0.85 HAT & 0.85 dECM) the organoids died due to cytotoxic materials, H_2O_2 at a too high concentration and EO Y. Therefore, the formulation of the ink was altered with a lower H_2O_2 concentration. Furthermore, EO Y was removed from the bioink to ensure the viability of organoids. The liver organoids stayed alive in the 0.51 dECM bioink for three days.

5.2. Recommendations

This study can be used as a foundation for comprehending the role of materials used in creating a human donor-derived bioink on printing and cytocompatibility. The next logical step for this project would be to 3D bioprint using the human donor-derived bioink developed in this project.

In the future, both the HAT and H_2O_2 concentrations should be reduced to make the ink less cytotoxic. The inks will become more fluid due to this variation. Therefore, to compensate for the less viscous ink, a higher dECM ratio should be added resulting in stiffer prints. The increase of human donor-derived liver dECM could be biologically significant as it would better recapitulate the *in vivo* liver environment, enhancing the organoids' viability and proliferation.

The effect of the components in the ink was investigated on organoids. The secondary post-crosslinking step with EO Y led to the ICOs death. To preserve the shape of the scaffolds post-printing, ruthenium with sodium persulfate was suggested as this photoinitiator is less cytotoxic to cells. Other parameters could also affect cell viability such as the handling of the ink. ICO death could be linked to the introduction of high shear forces when manually mixing the viscous inks with the ICOs (Fig. 2.4).

The ICO study was monitored over three days. A longer organoid culture would allow more biological readouts for example for revealing the presence of liver-specific genes with qPCR. Additionally, a longer study would be more relevant for liver disease modelling.

Tyramine-modified hyaluronic acid inks were formulated due to the physiological presence of HA in the human body but also for its tuneable stiffness [12]. Consequently, this bioink can be employed to create stiffer models replicating the properties of liver diseases. These models may be the first step to treating liver diseases as they can serve for drug development to evaluate drug toxicity and efficacy.

Most of the previous works used cell lines usually originating from animal species or cancers, and commercial inks for their printability and biocompatibility. These materials do not represent the liver physiology, and will never mimic the liver environment. Hence, the use of patient and human donor-derived biomaterials such as dECM and liver organoid offer a direct link with *in vitro* studies to the *in vivo* physiology. The work in the 3D bioprinting field with human-derived biomaterials could be applied to patient-specific studies. This study was an initial step in bringing scientific research closer to treating liver diseases. In the future, we hope to create a full-scale viable liver replacement, reducing the organ shortage for liver transplantation.

List of Figures

List of Tables

References

1. Asrani, S. K., Devarbhavi, H., Eaton, J. & Kamath, P. S. Burden of liver diseases in the world. *Journal of Hepatology* **70.** doi:10.1016/J.JHEP.2018.09.014 (2019).
2. Bodzin, A. S. & Baker, T. B. Liver Transplantation Today: Where We Are Now and Where We Are Going. *Liver Transplantatio* **24.** doi:10.1002/LT.25320 (2018).
3. Deo, K. A., Singh, K. A., Peak, C. W., Alge, D. L. & Gaharwar, A. K. Bioprinting 101: Design, Fabrication, and Evaluation of Cell-Laden 3D Bioprinted Scaffolds. *Tissue Engineering - Part A* **26.** doi:10.1089/ten.tea.2019.0298 (2020).
4. Lee, A. *et al.* 3D bioprinting of collagen to rebuild components of the human heart. *Science* **365.** doi:10.1126/science.aav9051 (2019).
5. Yeh, W.-c. *et al.* Elastic modulus measurements of human liver and correlation with pathology. *Ultrasound in Med. & Biol* **28.** doi:10.1016/S0301-5629(02)00489-1 (2002).
6. Yin, M. *et al.* Assessment of Hepatic Fibrosis With Magnetic Resonance Elastography. *Clinical Gastroenterology and Hepatology* **5.** doi:10.1016/J.CGH.2007.06.012 (2007).
7. Vermeulen, N., Haddow, G., Seymour, T., Faulkner-Jones, A. & Shu, W. 3D bioprint me: A socioethical view of bioprinting human organs and tissues. *Journal of Medical Ethics* **43.** doi:10.1136/medethics-2015-103347 (2017).
8. Loai, S., Kingston, B. R., Wang, Z. & Philpott, D. N. Clinical Perspectives on 3D Bioprinting Paradigms for Regenerative Medicine. *Regenerative Medicine Frontiers.* doi:10.20900/rmf20190004 (2019).
9. Sarkar, J., Kamble, S. C. & Kashikar, N. C. Polymeric Bioinks for 3D Hepatic Printing. *Chemistry* **3.** doi:10.3390/chemistry3010014 (2021).
10. Petta, D., Grijpma, D. W., Alini, M., Eglin, D. & D'este, M. Three-Dimensional Printing of a Tyramine Hyaluronan Derivative with Double Gelation Mechanism for Independent Tuning of Shear Thinning and Postprinting Curing. doi:10.1021/acsbiomaterials.8b00416 (2018).
11. Deegan, D. B., Zimmerman, C., Skardal, A., Atala, A. & Shupe, T. D. Stiffness of hyaluronic acid gels containing liver extracellular matrix supports human hepatocyte function and alters cell morphology. *Journal of the Mechanical Behavior of Biomedical Materials* **55.** doi:10.1016/J.JMBBM.2015.10.016 (2016).
12. Díaz-Payno, P. J. *et al.* Swelling-Dependent Shape-Based Transformation of a Human Mesenchymal Stromal Cells-Laden 4D Bioprinted Construct for Cartilage Tissue Engineering. *Advanced Healthcare Materials* **12.** doi:10.1002/ADHM.202201891 (2023).
13. Willemse, J., van der Laan, L. J. W., de Jonge, J. & Verstegen, M. M. A. Design by Nature: Emerging Applications of Native Liver Extracellular Matrix for Cholangiocyte Organoid-Based Regenerative Medicine. *Bioengineering* **9,** 110. doi:10.3390/BIOENGINEERING9030110 (2022).
14. Theocharis, A. D., Skandalis, S. S., Gialeli, C. & Karamanos, N. K. Extracellular matrix structure. *Advanced Drug Delivery Reviews* **97.** doi:10.1016/J.ADDR.2015.11.001 (2016).
15. Abaci, A. & Guvendiren, M. Designing Decellularized Extracellular Matrix-Based Bioinks for 3D Bioprinting. *Advanced Healthcare Materials* **9.** doi:10.1002/adhm.202000734 (2020).
16. Ali, M. *et al.* A Photo-Crosslinkable Kidney ECM-Derived Bioink Accelerates Renal Tissue Formation. *Advanced Healthcare Materials* **8.** doi:10.1002/adhm.201800992 (2019).
17. Mao, Q. *et al.* Fabrication of liver microtissue with liver decellularized extracellular matrix (dECM) bioink by digital light processing (DLP) bioprinting. *Materials Science and Engineering C* **109.** doi:10.1016/j.msec.2020.110625 (2020).

18. Jaramillo, M., Yeh, H., Yarmush, M. L. & Uygun, B. E. Decellularized human liver extracellular matrix (hDLM)-mediated hepatic differentiation of human induced pluripotent stem cells (hIPSCs). *Journal of tissue engineering and regenerative medicine* **12.** doi:10.1002/TERM.2627 (2018).

19. Lee, H. *et al.* Development of Liver Decellularized Extracellular Matrix Bioink for Three-Dimensional Cell Printing-Based Liver Tissue Engineering. *Biomacromolecules* **18.** doi:10.1021/acs.biomac.6b01908 (2017).

20. De Santis, M. M. *et al.* Extracellular-Matrix-Reinforced Bioinks for 3D Bioprinting Human Tissue. *Advanced Materials* **33.** doi:10.1002/adma.202005476 (2021).

21. Khati, V. *et al.* 3D Bioprinting of Multi-Material Decellularized Liver Matrix Hydrogel at Physiological Temperatures. *Biosensors* **12.** doi:10.3390/BIOS12070521 (2022).

22. Ma, X. *et al.* Rapid 3D bioprinting of decellularized extracellular matrix with regionally varied mechanical properties and biomimetic microarchitecture. *Biomaterials* **185.** doi:10.1016/j.biomaterials.2018.09.026 (2018).

23. Hiller, T. *et al.* Generation of a 3D Liver Model Comprising Human Extracellular Matrix in an Alginate/Gelatin-Based Bioink by Extrusion Bioprinting for Infection and Transduction Studies. *International journal of molecular sciences* **19.** doi:10.3390/IJMS19103129 (2018).

24. Kim, M. K. *et al.* Decellularized extracellular matrix-based bio-ink with enhanced 3D printability and mechanical properties. *Biofabrication* **12.** doi:10.1088/1758-5090/ab5d80 (2020).

25. Janani, G., Priya, S., Dey, S. & Mandal, B. B. Mimicking Native Liver Lobule Microarchitecture In Vitro with Parenchymal and Non-parenchymal Cells Using 3D Bioprinting for Drug Toxicity and Drug Screening Applications. *ACS Applied Materials and Interfaces* **14.** doi:10.1021/acsami.2c00312 (2022).

26. Jeong, W., Kim, M. K. & Kang, H. W. Effect of detergent type on the performance of liver decellularized extracellular matrix-based bio-inks. *Journal of Tissue Engineering* **12.** doi:10.1177/2041731421997091 (2021).

27. Mavri-Damelin, D. *et al.* Cells for bioartificial liver devices: The human hepatoma-derived cell line C3A produces urea but does not detoxify ammonia. *Biotechnology and Bioengineering* **99.** doi:10.1002/bit.21599 (2008).

28. Lu, S. *et al.* Recent advances in the development of in vitro liver models for hepatotoxicity testing. *Bio-Design and Manufacturing* **4.** doi:10.1007/S42242-021-00142-7 (2021).

29. Marsee, A. *et al.* Building consensus on definition and nomenclature of hepatic, pancreatic, and biliary organoids. *Cell Stem Cell* **28.** doi:10.1016/j.stem.2021.04.005 (2021).

30. Harrison, S. P. *et al.* Liver Organoids: Recent Developments, Limitations and Potential. *Frontiers in Medicine* **8.** doi:10.3389/fmed.2021.574047 (2021).

31. Norona, L. M., Nguyen, D. G., Gerber, D. A., Presnell, S. C. & LeCluyse, E. L. Modeling compound-induced fibrogenesis in vitro using three-dimensional bioprinted human liver tissues. *Toxicological Sciences* **154.** doi:10.1093/TOXSCI/KFW169 (2016).

32. Bouwmeester, M. C. *et al.* Bioprinting of Human Liver-Derived Epithelial Organoids for Toxicity Studies. *Macromolecular bioscience* **21.** doi:10.1002/mabi.202100327 (2021).

33. Nuñez Bernal, P. *et al.* Volumetric Bioprinting of Organoids and Optically Tuned Hydrogels to Build Liver-Like Metabolic Biofactories. *Advanced Materials.* doi:10.1002/ADMA.202110054 (2022).

34. Willemse, J. *et al.* Fast, robust and effective decellularization of whole human livers using mild detergents and pressure controlled perfusion. *Materials Science and Engineering C* **108.** doi:10.1016/j.msec.2019.110200 (2020).

35. Frayssinet, A. *et al.* Extracellular matrix-mimetic composite hydrogels of cross-linked hyaluronan and fibrillar collagen with tunable properties and ultrastructure. *Carbohydrate Polymers* **236.** doi:10.1016/j.carbpol.2020.116042 (2020).

36. Kurisawa, M., Chung, J. E., Yang, Y. Y., Gao, S. J. & Uyama, H. Injectable biodegradable hydrogels composed of hyaluronic acid–tyramine conjugates for drug delivery and tissue engineering. *Chemical Communications.* doi:10.1039/B506989K (2005).

37. Khanmohammadi, M. *et al.* Horseradish peroxidase-catalyzed hydrogelation for biomedical applications. *Biomaterials Science* **6.** doi:10.1039/c8bm00056e (2018).
38. Berkhout, W. E. M. *4D Bioprinting: Temporal Stiffening of Mesenchymal Stem Cell-Laden Hyaluronic Acid-Alginate Scaffolds for Cartilage Constructs* tech. rep. (Delft University of Technology, 2021).
39. Kalogeropoulou, M. *4D bioprinting for cartilage tissue engineering: a controlled shape transformation approach* tech. rep. (Delft University of Technology, 2021).
40. Kingma Esther. *The Development of a Cartilage Specific Bioink for Three-Dimensional Bioprinting* tech. rep. (Delft University of Technology, 2021).
41. *Viability/Cytotoxicity Assay Kit for Animal Live & Dead Cells (Calcein AM, EthD-1 Method) PF00008 | Proteintech*
42. King, A. P. & Eckersley, R. J. Descriptive Statistics I: Univariate Statistics. *Statistics for Biomedical Engineers and Scientists.* doi:10.1016/B978-0-08-102939-8.00010-4 (2019).
43. Hafizah, A. H. *et al.* Piper sarmentosum as an antioxidant on oxidative stress in human umbilical vein endothelial cells induced by hydrogen peroxide. *Journal of Zhejiang University: Science B* **11.** doi:10.1631/jzus.B0900397 (2010).
44. Teramoto, S. *et al.* Hydrogen peroxide-induced apoptosis and necrosis in human lung fibroblasts: protective roles of glutathione. *Japanese journal of pharmacology* **79.** doi:10.1254/JJP.79.33 (1999).
45. Bae, J. W., Choi, J. H., Lee, Y. & Park, K. D. Horseradish peroxidase-catalysed in situ-forming hydrogels for tissue-engineering applications. *Journal of Tissue Engineering and Regenerative Medicine* **9.** doi:10.1002/term.1917 (2015).
46. Raman, R. & Bashir, R. Stereolithographic 3D bioprinting for biomedical applications. *Essentials of 3D Biofabrication and Translation.* doi:10.1016/B978-0-12-800972-7.00006-2 (2015).
47. Kourouklis, A. P., Kaylan, K. B. & Underhill, G. H. Substrate stiffness and matrix composition coordinately control the differentiation of liver progenitor cells. *Biomaterials* **99.** doi:10.1016/j.biomaterials.2016.05.016 (2016).
48. Petta, D. *et al.* 3D bioprinting of a hyaluronan bioink through enzymatic-and visible light-crosslinking. *Biofabrication* **10.** doi:10.1088/1758-5090/aadf58 (2018).
49. Gudowska, M. *et al.* Hyaluronic acid concentration in liver diseases. *Clinical and Experimental Medicine* **16.** doi:10.1007/s10238-015-0388-8 (2016).
50. Neuman, M. G., Cohen, L. B. & Nanau, R. M. Hyaluronic acid as a non-invasive biomarker of liver fibrosis. *Clinical Biochemistry* **49.** doi:10.1016/j.clinbiochem.2015.07.019 (2016).
51. Müller, M., Öztürk, E., Arlov, Ø., Gatenholm, P. & Zenobi-Wong, M. Alginate Sulfate–Nanocellulose Bioinks for Cartilage Bioprinting Applications. *Annals of Biomedical Engineering* **45.** doi:10.1007/s10439-016-1704-5 (2017).
52. Nair, K. *et al.* Characterization of cell viability during bioprinting processes. *Biotechnology Journal* **4.** doi:10.1002/BIOT.200900004 (2009).
53. Shin, Y. J. *et al.* 3D bioprinting of mechanically tuned bioinks derived from cardiac decellularized extracellular matrix. *Acta Biomaterialia* **119.** doi:10.1016/J.ACTBIO.2020.11.006 (2021).
54. Cao, E., Chen, Y., Cui, Z. & Foster, P. R. Effect of freezing and thawing rates on denaturation of proteins in aqueous solutions. *Biotechnology and bioengineering* **82.** doi:10.1002/BIT.10612 (2003).
55. Cuhadar, S., Koseoglu, M., Atay, A. & Dirican, A. The effect of storage time and freeze-thaw cycles on the stability of serum samples. *Biochemia medica* **23.** doi:10.11613/BM.2013.009 (2013).
56. Shih, H. & Lin, C. C. Visible-light-mediated thiol-ene hydrogelation using eosin-Y as the only photoinitiator. *Macromolecular Rapid Communications* **34.** doi:10.1002/marc.201200605 (2013).
57. Bahney, C. S. *et al.* Visible light photoinitiation of mesenchymal stem cell-laden bioresponsive hydrogels. *European Cells and Materials* **22.** doi:10.22203/eCM.v022a04 (2011).
58. Camp, C. P. *et al.* Non-cytotoxic Dityrosine Photocrosslinked Polymeric Materials With Targeted Elastic Moduli. *Frontiers in Chemistry* **8.** doi:10.3389/fchem.2020.00173 (2020).

59. Lim, K. S. *et al.* New Visible-Light Photoinitiating System for Improved Print Fidelity in Gelatin-Based Bioinks. *ACS Biomaterials Science and Engineering* **2.** doi:10.1021/acsbiomaterials.6b00149 (2016).

60. Willemse, J. *et al.* Hydrogels derived from decellularized liver tissue support the growth and differentiation of cholangiocyte organoids. *Biomaterials* **284.** doi:10.1016/J.BIOMATERIALS.2022.121473 (2022).

61. Lee, H. *et al.* Cell-printed 3D liver-on-a-chip possessing a liver microenvironment and biliary system. *Biofabrication* **11.** doi:10.1088/1758-5090/aaf9fa (2019).

62. Bhise, N. S. *et al.* A liver-on-a-chip platform with bioprinted hepatic spheroids. *Biofabrication* **8.** doi:10.1088/1758-5090/8/1/014101 (2016).

63. Yi, S. A. *et al.* Bioengineering Approaches for the Advanced Organoid Research. *Advanced Materials* **33.** doi:10.1002/ADMA.202007949 (2021).

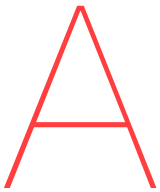

Composition Of Cell Culture Media

Table A.1: Composition of Cell Culture Media

Starting Medium (SM) Composition (Prepared weekly at Erasmus MC)

Component	Supplier	Cat. No.	µL.mL^{-1}	Final conc.
AdF12 +++	Gibco / ThermoFisher Scientific	12634028	852.2	
N2	Gibco / ThermoFisher Scientific	15410294	10	
B27	Gibco / ThermoFisher Scientific	12587001	20	
Gastrin I	Sigma-Aldrich	G9145	1	10 nM
FGF10	Peprotech	100-26	1	100 ng/ml
HGF	Tebu-Bio	167100-39-0500	1	25 ng/ml
EGF	Peprotech	AF-100-15	1	50 ng/ml
A8301 (Ti)	Cayman Chemical / Sanbio bv	9001799-25	1	5 µM
Nicotinamide	Sigma-Aldrich	N0636-100G	10	10 mM
Forskolin	Cayman Chemical / Sanbio bv	11018-50	1	10 µM
Ac Cys	Sigma-Aldrich	A9165-25G	2	1 mM
RSPo CM	Made at Erasmus MC	Conditioned medium	100	
Y27632	MedChem Express / Bioconnect	HY-10583_10mg	1	

Table A.2: Composition of Expansion Medium

Expansion Medium (EM) Composition (Prepared weekly at Erasmus MC)

Component	Supplier	Cat. No.	µL.mL^{-1}	Final conc.
AdF12 +++	Gibco / ThermoFisher Scientific	12634028	852.2	
N2	Gibco / ThermoFisher Scientific	15410294	10	
B27	Gibco / ThermoFisher Scientific	12587001	20	
Gastrin I	Sigma-Aldrich	G9145	1	10 nM
FGF10	Peprotech	100-26	1	100 ng/ml
HGF	Tebu-Bio	167100-39-0500	0.5	25 ng/ml
EGF	Peprotech	AF-100-15	1	50 ng/ml
A8301 (Ti)	Cayman Chemical / Sanbio bv	9001799-25	1	5 µM
Nicotinamide	Sigma-Aldrich	N0636-100G	10	10 mM
Forskolin	Cayman Chemical / Sanbio bv	11018-50	1	10 µM
Ac Cys	Sigma-Aldrich	A9165-25G	2	1 mM
RSPo CM	Made at Erasmus MC	Conditioned medium	100	

Table A.3: Composition of AdvDMEM/F12, Washing Buffer

AdvDMEM/F12 Composition (Prepared by Sleeboom J.)

Component	Supplier	Cat. No.	Final conc.
AdF12 +++	Gibco / ThermoFisher Scientific	11550446	
Primocin	Bio-Connect Life Sciences	Ant-Pm-2	0.2%
Hepes	Gibco / ThermoFisher Scientific	12509079	1%
Glutamax	Gibco / ThermoFisher Scientific	11574466	1%

B

Growth of ICOs

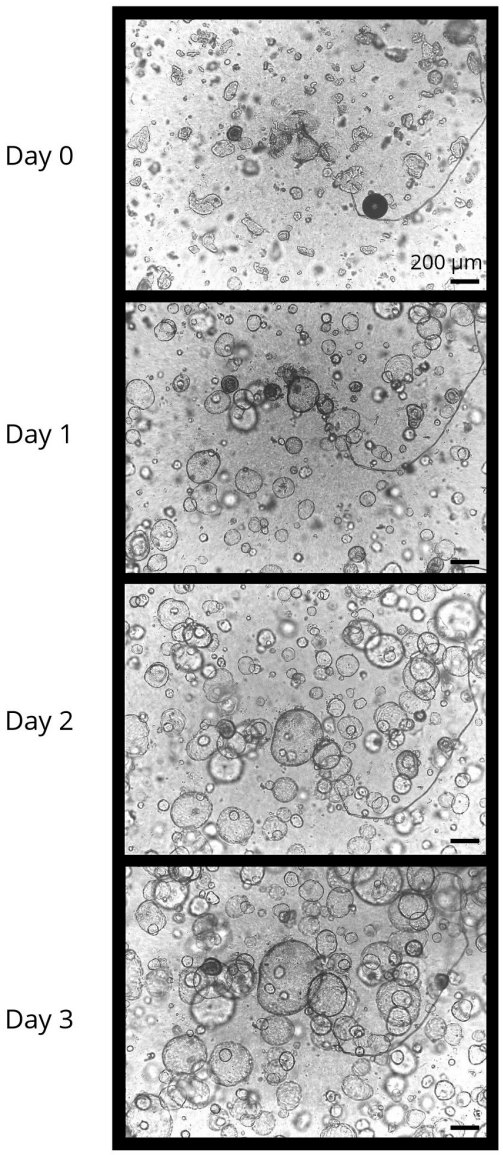

Figure B.1: Growth of ICOs in BME, from day 0 after splitting, day 1, day 2, and day 3. Scale Bars 200 µm

C

Toxicity of H_2O_2 for ICOs incorporated in BME

C.1. Methods

Two experiments were conducted to measure the toxicity of H_2O_2 present in the ink. The first experiment consisted plating ICOs contained in BME and adding different concentrations of H_2O_2 (0, 0.17, 0.51, and 0.85 mM) to the expansion medium. In the second experiment, 0.1 $U.mL^{-1}$ of HRP was added to the same concentrations of H_2O_2 used in the first experiment. The solutions were incubated for 30 min at 37°C in a similar way to the ink preparation. The ICOs were visually monitored over several days, and Live/Dead stainings were performed on day 3.

C.2. Results

C.2.1. H_2O_2 supplemented to EM

From day 1, ICOs in the EM containing 0.85 mM H_2O_2 were fragmented (Fig.C.1). The Live/Dead stainings in Fig.C.2 confirmed cell death. The growth of the ICOs was not significantly impacted in the 0.17 mM and 0.51 mM H_2O_2 concentrations, from day 1 to day 2. The Live/Dead staining showed alive organoids. However, in the background of the stainings for the 0.51 mM H_2O_2 medium some cellular death was observed. The results indicated that high concentrations of H_2O_2 were cytotoxic for the ICOs.

C.2.2. H_2O_2 + HRP incubated & supplemented to EM

Under different H_2O_2 concentrations, ICOs grew from day 1 to day 2 (Fig.C.3). The Live/Dead staining on day 3 confirmed the viability of the ICOs in 0.17, 0.51, and 0.85 mM H_2O_2. The qualitative data implies that H_2O_2 and HRP reacted within 30 min at 37°C. These results suggest that 0.85 mM H_2O_2 was less cytotoxic to ICOs.

C.3. Conclusion & Discussion

These two experiments proved the cytotoxicity of H_2O_2. The second experiment aimed to determine if the HRP and H_2O_2 were consumed, resulting in a less cytotoxic environment for the ICOs. Nevertheless, the observed reaction with the HRP and H_2O_2 was different from the reaction in the ink, as the main component, HAT was absent. Additionally, these experiments did not replicate the conditions of the incorporation of ICOs in the ink, as the ICOs were not in direct contact with H_2O_2, and the BME may shield them from a cytotoxic reaction. Therefore, in the rest of the project, a concentration lower than 0.85mM H_2O_2 was selected.

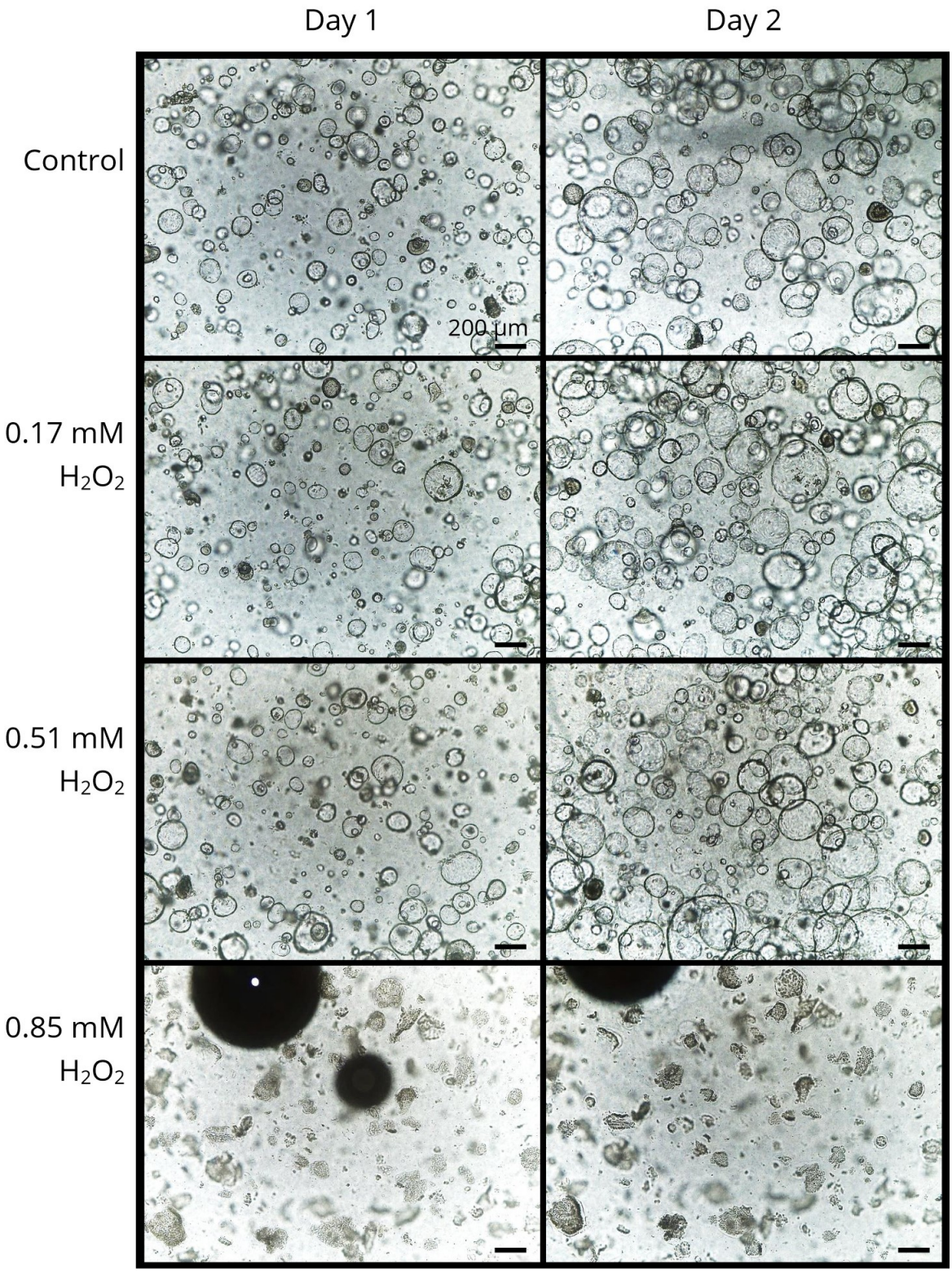

Figure C.1: Growth monitored and visualised over day 1 and day 2 of ICOs contained in BME supplemented with EM and different concentrations of H_2O_2. Scale Bars 200 µm

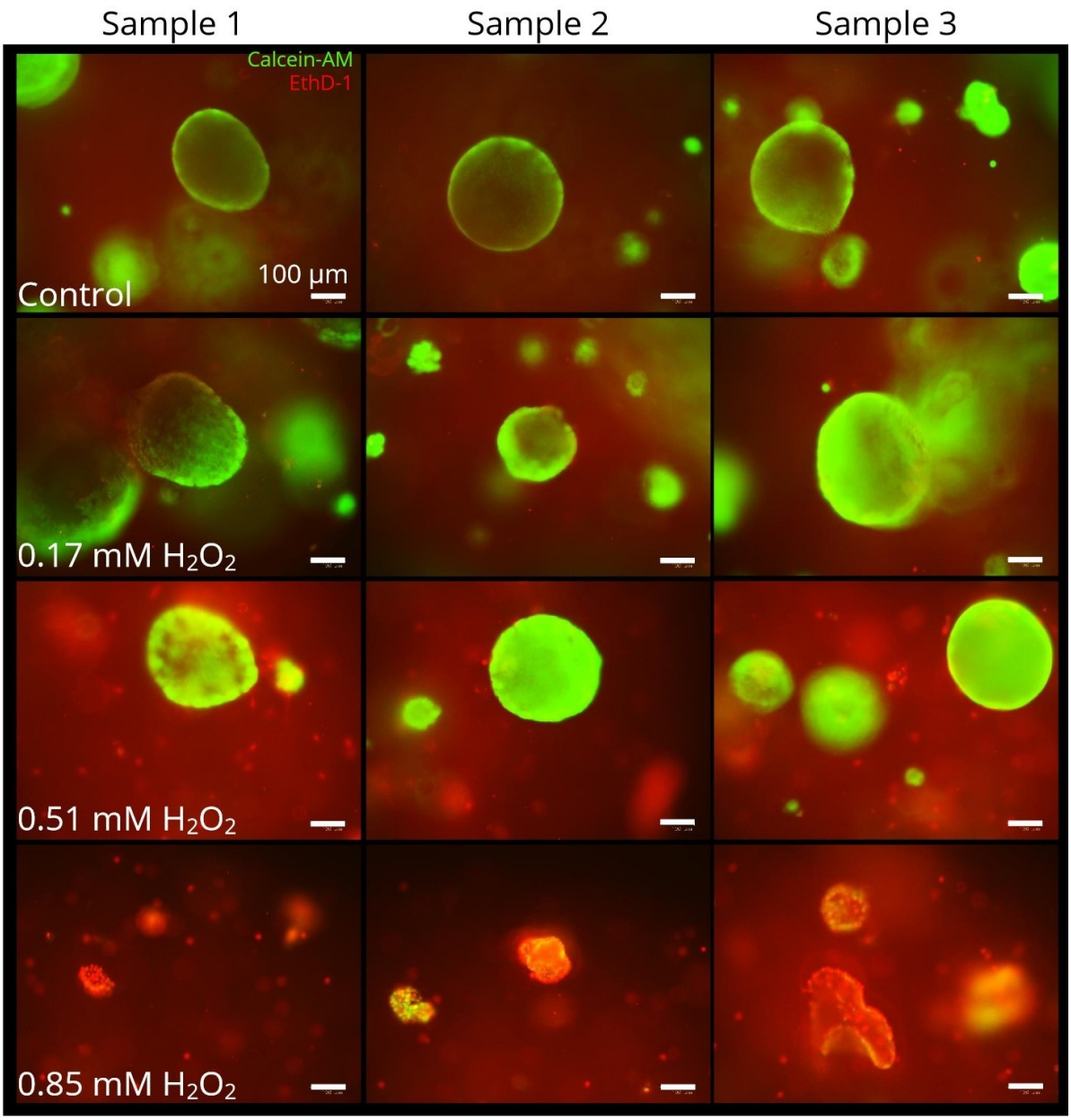

Figure C.2: Live/Dead staining on ICOs contained in BME supplemented with an EM containing different H_2O_2 concentrations. Scale Bars 100 µm

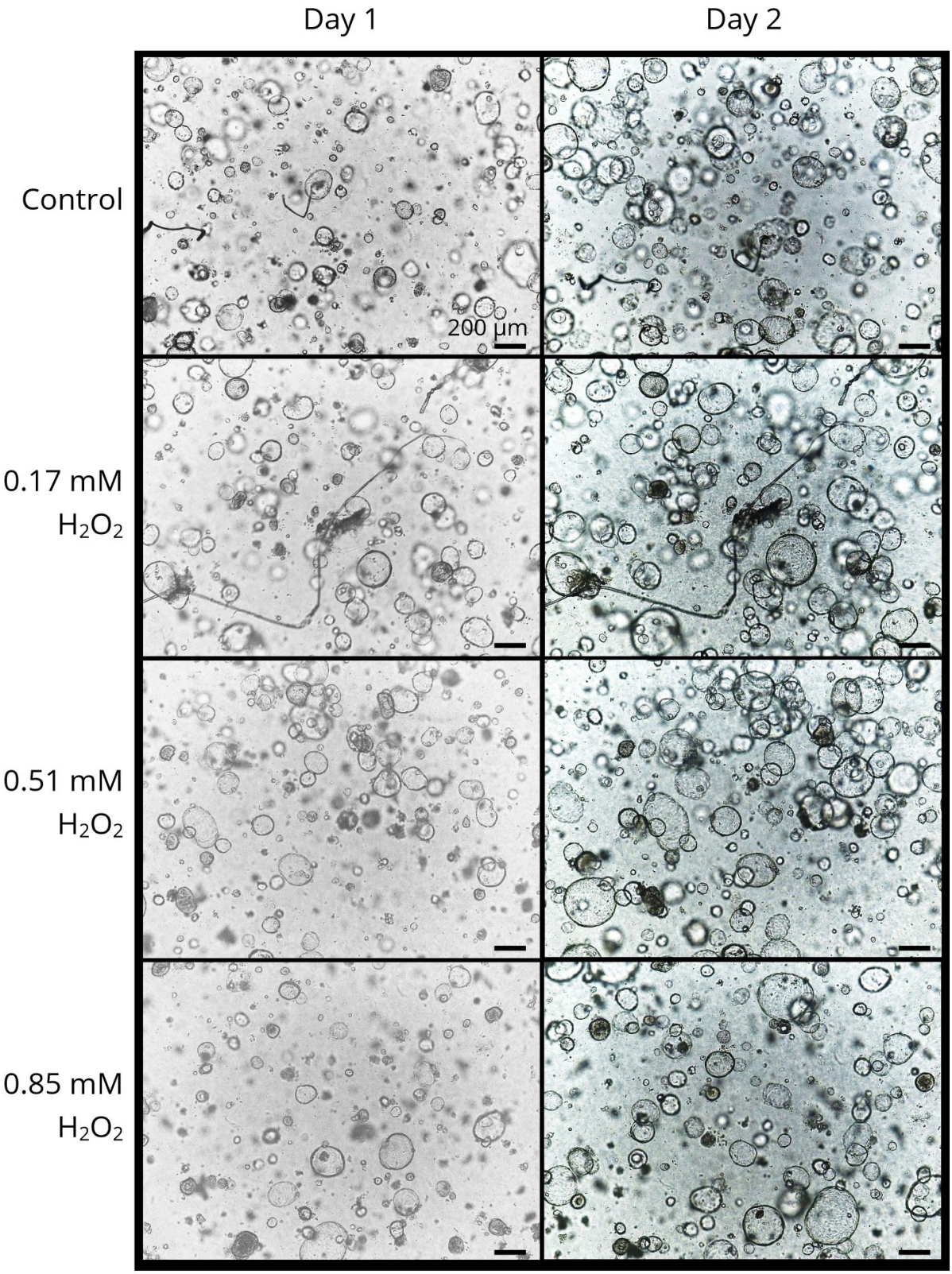

Figure C.3: Growth monitored and visualised over day 1 and day 2 of ICOs contained in BME supplemented with incubated expansion medium, HRP, and different concentrations of H_2O_2. Scale Bars 200 µm

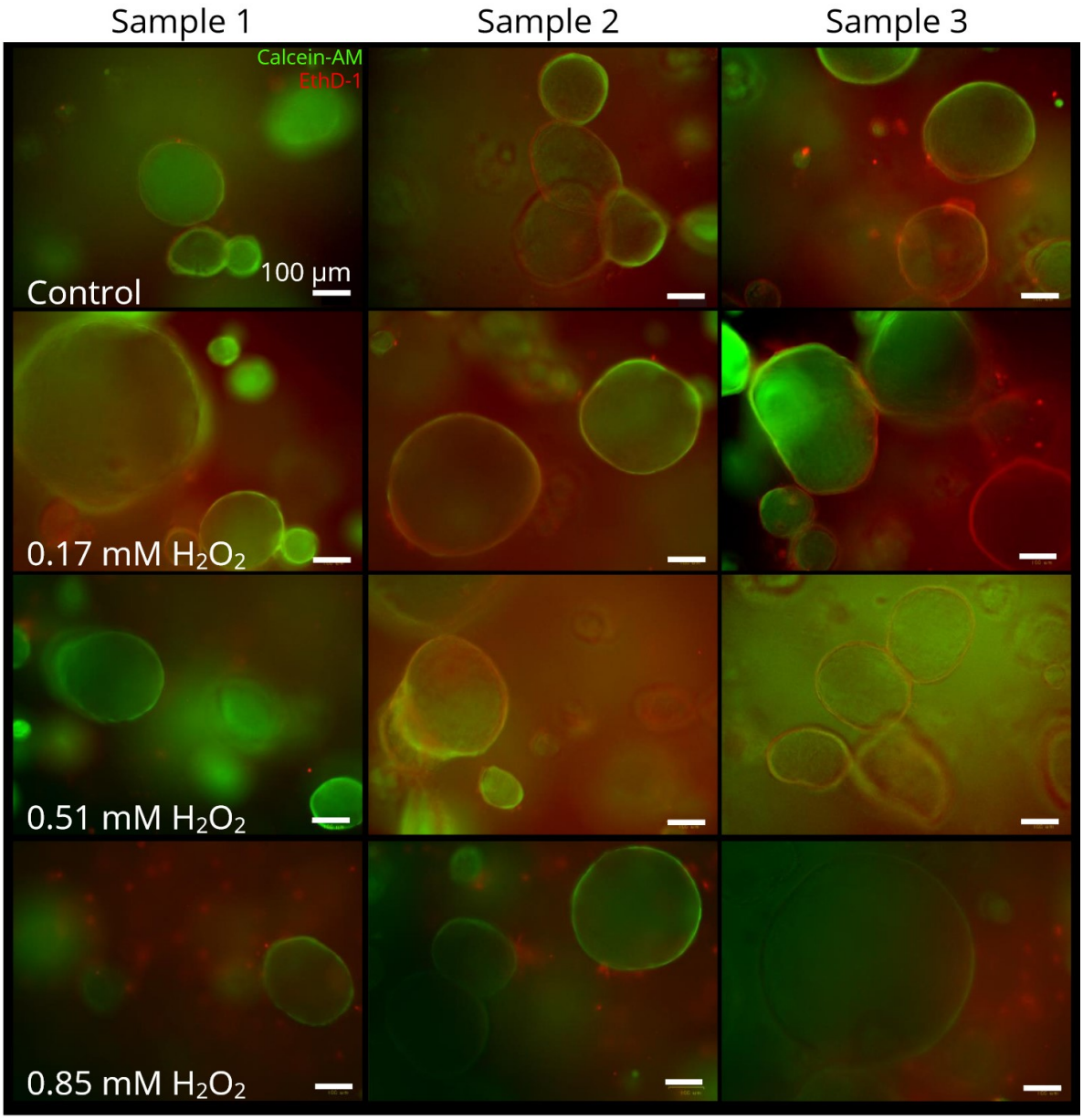

Figure C.4: Live/Dead staining on ICOs contained in BME supplemented with incubated expansion medium, HRP, and different concentrations of H_2O_2 concentrations. Scale Bars 100 µm

D

Toxicity of EO Y for ICOs incorporated in 0.51 dECM ink

D.1. Methods

For mechanical integrity of printed scaffolds, EO Y (0.01% v/v) was added in the ink and post-bioprinting photo-crosslinked with visible green light for 5 min on each side of the well plate. The influence of EO Y on the ICOs was investigated, in this experiment. ICOs were introduced to the 0.51 dECM ink according to Protocol 2.4.

D.2. Results

From Figure D.1 from day 1 to day 3 ICOs were added in the 0.51 dECM ink. The presence of EO Y was confirmed by the pink coloration. However, from day 1 to day 3, there was no observed organoid growth. The Live/Dead staining revealed in red the cell death of ICOs. Based on these findings, the photoinitiator was removed from the bioink formulation as a contributing factor to cytotoxicity.

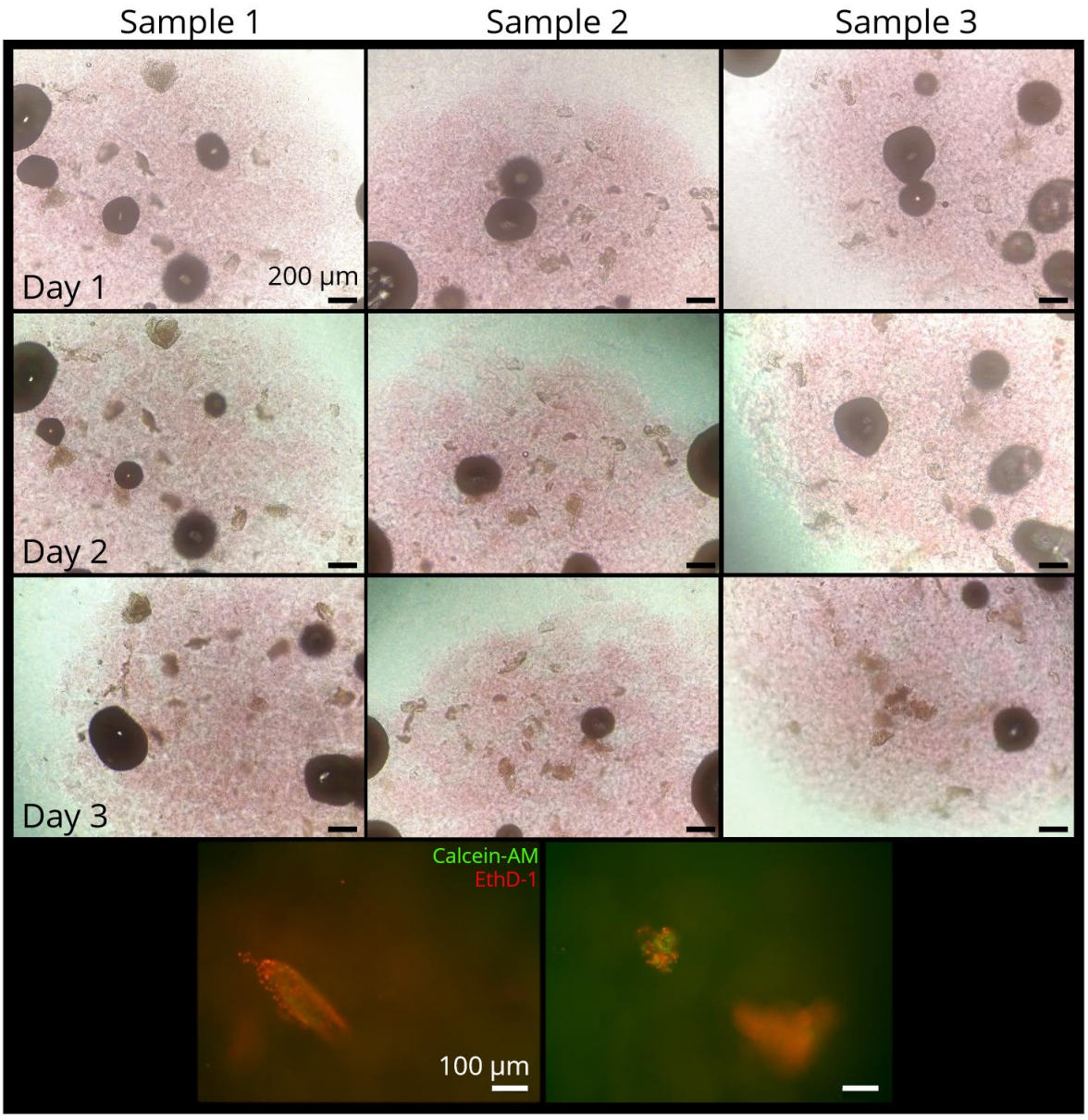

Figure D.1: ICOs in 0.51 dECM with 0.01% EO Y imaged on day 1, day 2, and day 3. Live/Dead staining of the 0.51 dECM + EO Y bioink on day 3. White Scale Bars 100 µm, Black Scale Bars 200 µm

E

Type I Collagen Staining

Liver dECM is composed of proteins where collagen Type I and Type III are the most abundant [60]. To prove the presence and distribution of the liver dECM in the 0.51 mM dECM ink, immunofluorescence stainings for Type I collagen were performed. The stainings were not included in the Results (Section 3) as the positive control was inconclusive.

E.1. Methods

Immunofluorescence staining is a type of assay for biological samples used to identify and locate specific biological components in a sample. Two antibodies were used for the Type I collagen staining. The primary antibody binds to the antigen of interest (Type I collagen). Then, the second antibody is added with a tagged fluorescent dye that is excited and visible under a fluorescent microscope if the antigen of interest is present in the sample. The process for immunofluorescence staining is shown in Fig.E.1.

The Type I collagen staining was done after the Live/Dead staining on day 3. The samples were air-dried overnight. First the primary antibody, anti-collagen I was diluted in 1x PBS at a ratio of 1:200 and added to the dehydrated samples. The samples were left in the incubator for 1 hour at 37^{o}C. The samples were washed in 1x PBS 3 times for 5 min at room temperature. The second antibody AlexaFluor 488 anti-rabbit was diluted in 1x PBS at a ratio of 1:200 and added to the samples of interest, which were placed in the incubator at 37^{o}C for 1 hour. The samples were rinsed with 1x PBS 3 times for 5 min at room temperature. Finally, a fluorescent microscope with an excitation wavelength of 495 nm (Zoe Fluorescent Cell Imager, BioRad, Hercules, California, U.S.A.) was used to capture the images of the samples.

E.2. Results

Fig.E.2 shows the stainings obtained for the 0.51 dECM ink. The Type I collagen staining was done on bioprinted samples (n=2), on day 3 after printing.

A fluorescent green signal was detected (Fig.E.2). Some of the arrows may point to some Type I collagen content. Additionally, some artifacts resembling butterflies can be seen in the background. These artifacts may have been a result of the air-drying process and may be NaCl crystals contained in the ink.

As the positive control was inconclusive, the results obtained from the scaffolds do not verify the presence of Type I collagen, and thus dECM presence in the scaffold.

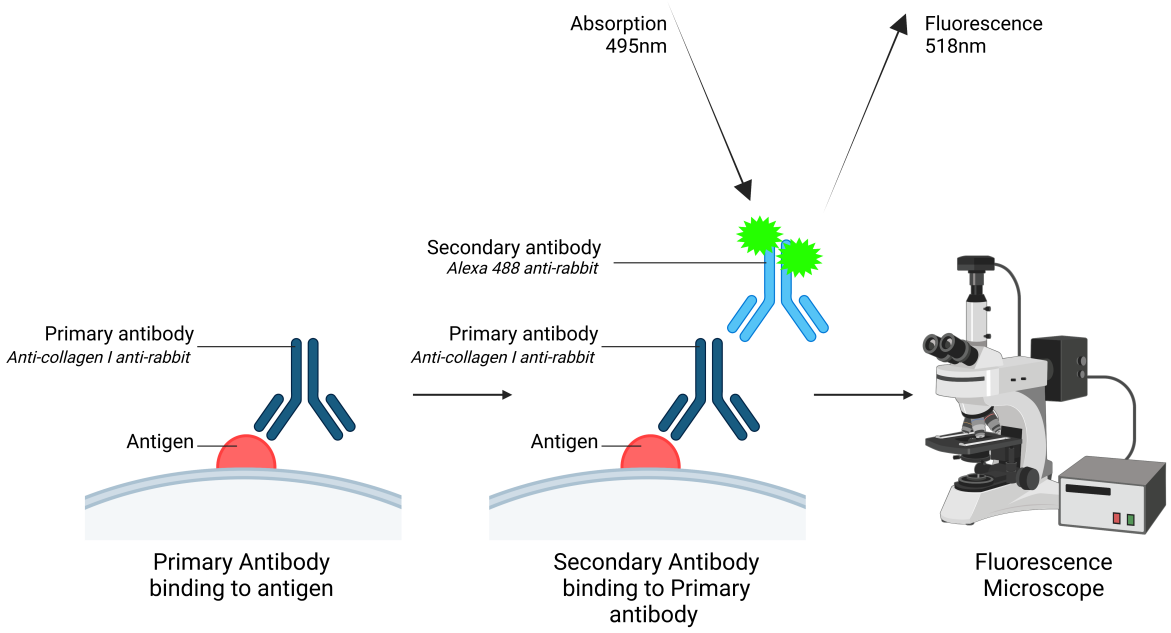

Figure E.1: Graphical illustration of the immunofluorescence staining protocol, for Type I collagen antibodies

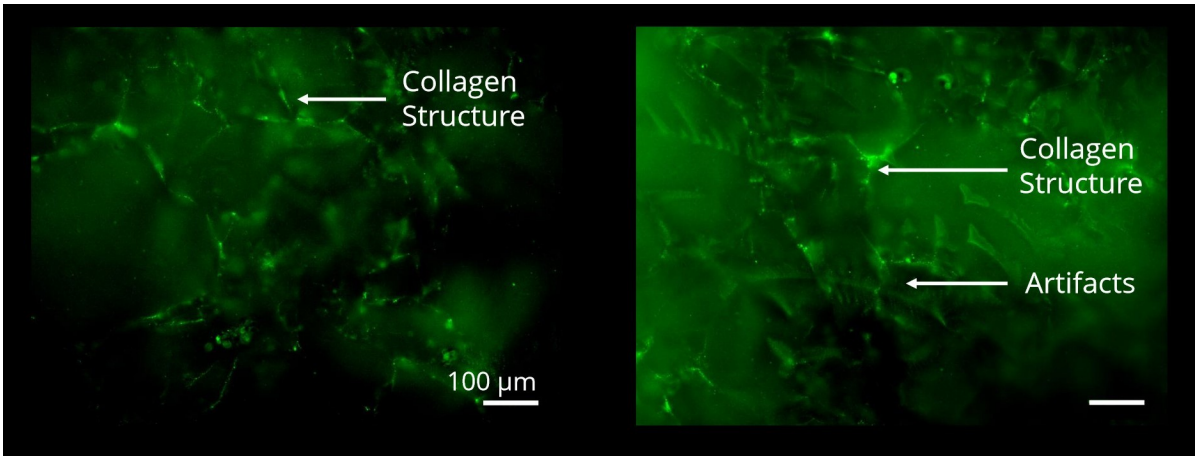

Figure E.2: Type I collagen staining on 0.51 dECM ink, done days post-printing. Scale Bars 100 µm

TU Delft

Erasmus MC
Universitair Medisch Centrum Rotterdam

A Promethean Construct

Flora Guarnotta